

Machine versus Human Attention in Deep Reinforcement Learning Tasks

Ruohan Zhang¹ Sihang Guo¹ Bo Liu¹ Yifeng Zhu¹ Dana Ballard¹ Mary Hayhoe² Peter Stone^{1,3}

Abstract

Deep reinforcement learning (RL) algorithms are powerful tools for solving visuomotor decision tasks. However, the trained models are often difficult to interpret, because they are represented as end-to-end deep neural networks. In this paper, we shed light on the inner workings of such trained models by analyzing the pixels that they attend to during task execution, and comparing them with the pixels attended to by humans executing the same tasks. To this end, we investigate the following two questions that, to the best of our knowledge, have not been previously studied. 1) How similar are the visual features learned by RL agents and humans when performing the same task? and, 2) How do similarities and differences in these learned features explain RL agents' performance on these tasks? Specifically, we compare the *saliency maps* of RL agents against visual attention models of human experts when learning to play Atari games. Further, we analyze how hyperparameters of the deep RL algorithm affect the learned features and saliency maps of the trained agents. The insights provided by our results have the potential to inform novel algorithms for the purpose of closing the performance gap between human experts and deep RL agents.

1. Introduction

Researchers have devoted much effort to understanding deep neural networks (DNNs). Since DNNs are partially inspired by the biological nervous systems, researchers have compared these neural networks with human brain and sensory systems by asking two typical types of questions. The first one considers representation: How similar are the visual features learned by DNNs and humans when performing the same tasks? The second one concerns explainability:

How do similarities and differences in these learned features explain DNNs' performance on their tasks?

The first question motivates a seminal line of research that compares features learned by DNNs with features learned by brains. In computer vision, a linear relation has been found between features learned by convolutional neural networks layers and neural responses of visual cortex (Eickenberg et al., 2017; Yamins et al., 2013; 2014). In language learning, a similar connection has been found between deep language models and cortical areas (Huth et al., 2016; Jain & Huth, 2018). However, this type of comparison has just emerged in decision-making research (Merel et al., 2019; Cross et al., 2020), which motivates us to compare DNNs trained for deep reinforcement learning (RL) tasks with human decision-making. In particular, we ask: For a given task, do deep RL agents and humans agree on what visual features are important? In other words, do agents pay *attention* to the same visual features as humans do?

The explainability question is motivated by the Explainable AI (XAI) paradigm for deep RL agents (Heuillet et al., 2020; Alharin et al., 2020; Puiutta & Veith, 2020). Deep RL agents still make mistakes, which researchers are interested in providing explanations for. However, these agents often learn a mapping from raw images to an action end-to-end where it is not clear why a particular decision is made. Our work addresses the explainability of these black-box models: Do RL agents make mistakes because they fail to attend to important visual features that matter for making the correct decision? An expert human's attention data could serve as a useful reference for identifying important visual features, which has been validated in computer vision research for object recognition tasks (Muddamsetty et al., 2021).

To answer these two questions, we situate our research in the domain of Atari games (Bellemare et al., 2013). These games span a variety of dynamics, visual features, reward mechanisms, and difficulty levels for both humans and AIs. Two recent lines of research have made our work possible. On the one hand, tools have been introduced to generate visual interpretations of RL agents (Greydanus et al., 2018). Through these tools, one can visualize an RL agent's *saliency map* given an image, which is a topographically arranged map that assigns an importance weight to each image pixel and is often treated as the "attention map" of

¹Department of Computer Science, The University of Texas at Austin ²Center for Perceptual Systems, The University of Texas at Austin ³Sony AI. Correspondence to: Ruohan Zhang <zharu@utexas.edu>.

the RL agent. On the other hand, a human attention dataset on Atari games has been collected using eye trackers (Zhang et al., 2020b), which makes a comparison study feasible.

In this work, We present the first study that compares human attention with the RL agent’s attention. We analyze how learning and hyperparameters of the RL algorithm affect the learned features and saliency maps. We show that RL agents make mistakes partly because they fail to attend to the correct visual targets. We further study whether RL agents’ attention generalizes to states that these agents have never visited. We conclude by discussing insights gained for RL researchers in both cognitive science and AI.

2. Related Work

Human vs. machine attention in vision and language tasks. Human expert’s gaze is very efficient and accurate for solving vision tasks. The peak angular speed of the human eye during a saccade (fast, jumping eye movement) reaches up to 900 degrees per second (Robinson, 1964). This allows humans to move their foveae to the right place at the right time to attend to important features (Diaz et al., 2013). Therefore, human expert’s gaze serves as a good standard in many vision-related tasks for evaluating machine attention, or as a learning target for training machine attention (Qiuxia et al., 2020; Zhang et al., 2020a). This approach is widely used in computer vision, see Nguyen et al. (2018) for a review.

For example, visual saliency researchers train DNNs to predict human visual attention. Saliency research is a well-developed field and we direct interested readers to recent review papers (Borji et al., 2015; Bylinskii et al., 2016; He et al., 2019a; Bylinskii et al., 2019). One such paper has compared visual saliency models with human visual attention (Lai et al., 2019). In vision-related language tasks, such as image captioning and visual question answering, it was found that the saliency maps of DNN models are different from human attention (Das et al., 2017; Tavakoli et al., 2017; He et al., 2019b). Understanding and quantifying such differences have provided insights on the performance, especially in failure scenarios, of these vision-language models.

Visual explanation for deep RL. Two classes of methods are widely used to generate visual interpretations of DNNs in the form of saliency maps: *gradient-based* and *perturbation-based*. Gradient-based methods compute saliency maps by estimating the input features’ influence on the output using the gradient information (Simonyan et al., 2013; Springenberg et al., 2014; Mahendran & Vedaldi, 2016; Zhang et al., 2018a; Shrikumar et al., 2017; Sundararajan et al., 2017; Selvaraju et al., 2017; Chattopadhyay et al., 2018; Zhou et al., 2016). These methods are for visualizing general DNNs but have been used to interpret deep RL agents (Joo & Kim, 2019; Weitkamp et al., 2018; Shi et al., 2020; Jaunet et al.,

2019; Wang et al., 2018). We did not use gradient-based saliency maps for our analysis because they lack physical meaning and could be difficult to interpret.

Perturbation-based methods alter parts of the input image and measure how much the output is affected by the change. Hence there have been different methods of alternating the input (Zeiler & Fergus, 2014; Fong & Vedaldi, 2017; Dabkowski & Gal, 2017; Zintgraf et al., 2017; Ribeiro et al., 2016). These methods have been applied to Atari deep RL agents and can generate qualitatively meaningful saliency maps (Greydanus et al., 2018; Iyer et al., 2018; Grimm et al., 2017; Puri et al., 2019). However, without human attention as a reference, it is difficult to quantitatively analyze these saliency maps, which motivates our work.

There are also methods that change the architecture of the deep RL network by augmenting it with an explicit artificial attention module, so that one can directly access its attention map (Mousavi et al., 2016; Yang et al., 2018; Mott et al., 2019). Researchers have taken this approach and compared RL agents’ attention with human attention (Nikulin et al., 2019). However, these methods do not apply to general deep RL algorithms since they need to modify the original network architectures and retrain the new ones.

Human visual attention data in decision-making tasks. Human visual attention data is often obtained using eye-trackers to record their eye movements (gaze). Recently, researchers have collected large-scale human gaze and decision datasets in several visuomotor tasks, such as meal preparation (Li et al., 2018), human-to-human social interactions (Zuo et al., 2018), driving (Palazzi et al., 2018), and Atari game playing (Zhang et al., 2020b). So far these datasets have been used for modeling human attention. Our work suggests a new possibility of using human attention data as a reference to visually interpret RL agents.

3. Method

We now discuss our approaches for obtaining the human attention model, training RL agents, and extracting attention information from the trained RL agents. We then discuss how we select data for comparing human versus RL attention, and define the comparison metrics.

3.1. Human attention data and model

We use human expert gaze data from Atari-HEAD dataset (Zhang et al., 2020b). The original game runs continually at 60Hz (Bellemare et al., 2013), a speed that is challenging even for professional gamers. Human eye movements were rushed and inaccurate at this speed hence could not serve as a useful reference. In Zhang et al. (2020b), however, the human data were collected in a semi-frame-by-frame mode, a design that allowed enough time for the play-

ers to attend to all relevant objects on the screen and make decisions. The slowed speed allowed players to achieve world expert level performance (Zhang et al., 2020b).

To get human saliency maps for the data generated by RL agents, we need an accurate human attention model. We did not use human states due to a state distribution mismatch. RL agents make many more mistakes than humans and cannot reach the late stages of the games like human experts. This creates a state distribution that does not match human data, which contains mostly good states. Having a human attention model allows us to perform comparisons in states encountered by RL agents only which is especially important when we later analyze RL agents’ failure states.

Predicting human attention is a challenging task in Atari games. The human gaze is rarely on the player’s avatar or contingency regions (Bellemare et al., 2013) so simple object detectors would not work. Human players often select and focus on a few among multiple visually identical objects, and divide their attention if multiple objects are relevant for decision making. Recently, variants of convolution-deconvolution network models have achieved the best results on predicting human attention from gaze data (Li et al., 2018; Zhang et al., 2018b; Palazzi et al., 2018; Deng et al., 2019). Here we follow their approach to train models with human gaze data to produce saliency maps as the ground truth.

As a control analysis, we include two attention models in addition to human gaze. The first one captures the motion information, measured by Farneback optical flow between two consecutive images (Farneback, 2003). The second model captures salient low-level image features, including color, orientation, and intensity (weighted equally), computed by the classic Itti-Koch saliency model (Itti et al., 1998).

3.2. Reinforcement learning agent and attention model

As a case study, we use a popular deep RL algorithm named Proximal Policy Optimization (PPO) (Schulman et al., 2017) with default hyperparameters (Hill et al., 2018). For each experimental condition (discussed later), we train 5 models with different random seeds. For the Atari gaming environment, we use the basic version that has no frame skipping and no stochasticity in action execution (NoFrameskip-v4 version). We select six popular Atari games.

We use a perturbation-based method (Greydanus et al., 2018) to extract attention maps from PPO agents, which has been validated by several subsequent studies (Gupta et al., 2019; Shi et al., 2020). The algorithm takes an input image I and applies a Gaussian filter to a pixel location (i, j) to blur the image. This manipulation adds spatial uncertainty to the region around and produces a perturbed image $\Phi(I, i, j)$. A saliency score for this pixel (i, j) can be defined as how

much the blurred image changes the policy π :

$$S_{\pi}(i, j) = \frac{1}{2} \|\pi(I) - \pi(\Phi(I, i, j))\|^2 \quad (1)$$

Instead of calculating the score for every pixel, (Greydanus et al., 2018) found that computing a saliency score for pixel $i \bmod 5$ and $j \bmod 5$ produced good saliency maps at lower computational cost for Atari games. The final saliency map P is normalized as $P(i, j) = \frac{S_{\pi}(i, j)}{\sum_{i, j} S_{\pi}(i, j)}$.

3.3. Comparison metrics

Next, we compile a set of game images to compute human and RL saliency maps. For each game, we let a trained PPO agent (with default hyperparameters) play the game until terminated, and uniformly sampled 100 images from the recorded trajectory. We will refer to this set of images as the standard image set.

We then define two metrics for comparing saliency maps: Pearson’s Correlation Coefficient (CC) and Kullback-Leibler Divergence (KL). Let Q denote the human saliency map predicted by the human attention network. CC is between -1 and 1 captures the linear relation between two distributions Q and P :

$$CC(P, Q) = \frac{\sigma(P, Q)}{\sigma_P \times \sigma_Q} \quad (2)$$

where $\sigma(P, Q)$ denotes the covariance, and σ_P and σ_Q are the standard deviations of P and Q respectively. CC penalizes false positives and false negatives equally.

However, we may not want to penalize the RL agent if it attends to regions that the human gaze model is not currently focused on. The human gaze data only reveals their “overt” attention, and humans can still pay “covert” attention to entities in the working memory (Posner, 1980; Saran et al., 2020). In other words, being attended by the human gaze is a sufficient (but not necessary) condition for the features to be important. Thus we need a second metric that penalizes the agent only if it *fails* to pay attention to human attended regions, or equivalently, a metric that is sensitive to false negatives if we treat human attention as the ground truth. KL is an ideal candidate in this case (Bylinskii et al., 2019):

$$KL(P, Q) = \sum_i \sum_j Q(i, j) \log \left(\epsilon + \frac{Q(i, j)}{\epsilon + P(i, j)} \right) \quad (3)$$

where ϵ is a small regularization constant (chosen to be $2.2204e-16$ (Bylinskii et al., 2019)) and determines how much zero-valued predictions are penalized.

4. Results

To make meaningful comparisons, we first ensure that the human attention model is accurate, and PPO agents’ at-

tention maps are consistent over repeated runs. We then compare human attention with PPO attention that is obtained from different learning stages and from agents that are trained with different discount factors. We then analyze PPO agents’ attention in failure and unseen states. At last, we show comparison results for other deep RL algorithms.

Accuracy of human attention model We implement the convolution-deconvolution gaze prediction network (Zhang et al., 2020b) to generate a human saliency map for image I_t at timestep t , given a stack of four consecutive images $I_{t-3}, I_{t-2}, I_{t-1}, I_t$ as input. We use 80% gaze data for training and 20% for testing. The network model can accurately predict the human gaze. On testing data, we obtained Area under ROC Curve (AUC) score of 0.968 ± 0.005 , CC of 0.562 ± 0.030 , and KL of 1.411 ± 0.114 ($n = 6$), averaged over all games. Prediction accuracy for individual games can be found in Appendix 1 of the supplementary materials. A visualization of the gaze data and prediction results can be found in the attached video file. The accuracy is considered high in saliency research (Bylinskii et al., 2019).

Consistency of RL attention We then show that saliency maps of the RL agents trained under the same experiment setting, provided by Hill et al. (2018), are highly consistent, despite the stochasticity in the training process. The stochasticity is controlled by a random seed which is used to initialize both the game environment and the network. For each game, we use 5 random seeds (0-4), train an agent using each seed, and generate 5 saliency maps with these trained agents. For each image in the standard set, we compute pair-wise CCs between these 5 saliency maps (10 CCs in total). The average value for these 10 CCs, across 100 images and 6 games, is $0.924(\pm 0.001, n = 6000)$. Given such high consistency, the saliency maps we use later are the averaged results of these 5 saliency maps.

4.1. RL versus human attention: The effects of learning

So far we have verified that the gaze model can accurately predict human attention and that RL attention is consistent across repeated runs. We now address the primary research question: How similar are the visual features learned by RL agents and humans when performing the same task? We first study how the attention of PPO agents evolves over time, compared with human attention. For each game, we saved neural network weights at different time steps during training. Then we use these saved models to generate saliency maps on the standard image set.

Fig. 1 shows the aggregated results for all games. CC values and (negative) KL values between human and RL increase during learning, indicating that the RL agents’ attention gradually becomes more human-like. We visualize the change of RL attention and human attention in Fig. 2. Net-

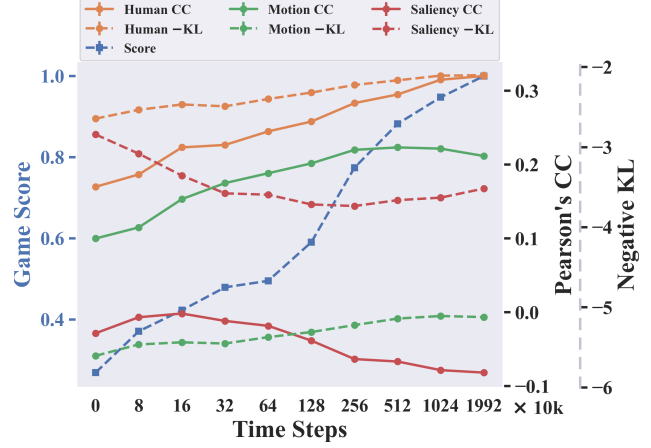


Figure 1. Changes in human and RL attention similarity across learning time steps. PPO agents gradually learn to pay attention to important visual features and develop become more human-like. We also show two control attention models: motion (optical flow) and saliency (low-level image features). The x-axis is log scale and KL values are negated for better visualization. The CC, KL, and score results for individual games, as well as more examples, can be found in Appendix 2.

works without any training (time step 0) have saliency maps that are positively correlated with humans ($CC = 0.170$). For example, the second column in Fig. 2 shows that these networks are already sensitive to low-level salient visual features without any learning, which is consistent with previous findings (Yamins et al., 2014; Greydanus et al., 2018). After training, human and RL saliency maps are more positively correlated ($CC = 0.320$), meanwhile RL and human are more similar to each other than the control models (higher CC/-KL values after training).

We also show aggregated game performance in normalized game scores in Fig. 1. For each game, we normalize the game scores obtained during learning (averaged over 50 episodes) by dividing them by the final scores. We find a strong positive correlation between the human CC/KL values and the game score (average Pearson’s correlation coefficient of $0.813/0.790$). The correlations for all games are statistically significant ($p < 0.05$, Appendix 2), indicating that small changes in similarity with human attention are reliable predictors of performance change. For comparison, the correlation values between CC/KL and game score for motion baseline are $0.404/0.251$, for saliency baseline are $-0.258/-0.688$.

This result sheds light on an important attention research topic: bottom-up versus top-down attention. The two sides debate how much human or machine attention is driven by bottom-up image features captured by the saliency model (Itti et al., 1998), and how much it is driven by top-down task signals such as reward (Rothkopf et al., 2007;

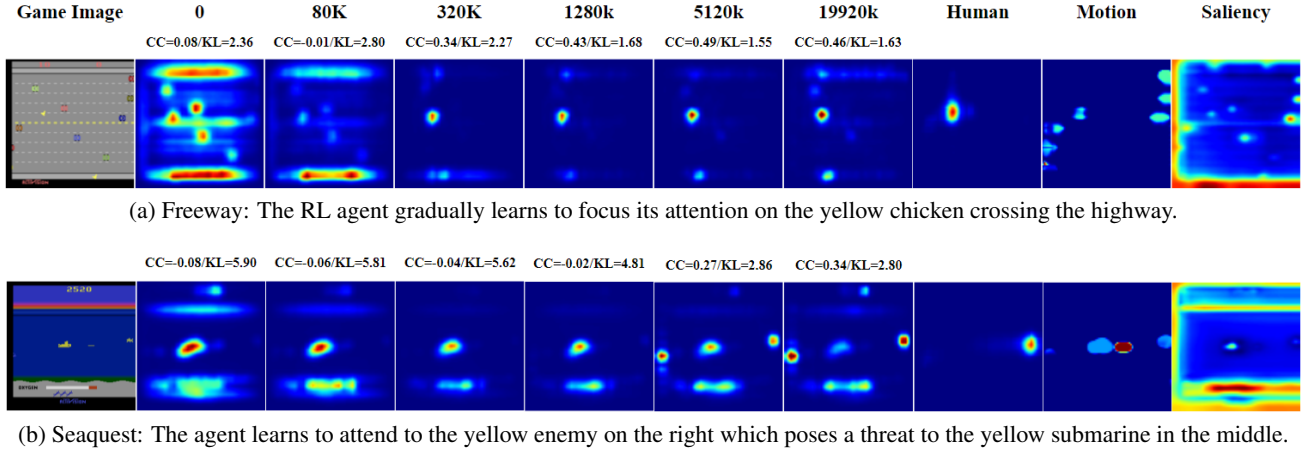


Figure 2. Attention of RL agents changes during learning and becomes more human-like. CC/KL values are calculated between the RL agent’s attention map and the human attention map.

Borji & Itti, 2014). Our result suggests that learning is a key factor in this debate. In the early stages, attention is more driven by image features, indicated by the higher similarity between RL attention and saliency baseline at the beginning. Then top-down reward signals shape the attention during learning by making reward-associated objects more salient and irrelevant objects less salient, as shown in Fig. 2.

4.2. RL versus human attention: Discount factors

We then analyze how hyperparameters of the PPO algorithm affect the attention of the trained agents. We have seen that reward shapes attention during training, therefore a reasonable hypothesis is that varying reward-related parameters will likely affect attention. The parameter we can vary in these games is the discount factor $\gamma \in [0, 1]$, which determines how much the RL agent weighs future reward compared to immediate reward. The default γ is 0.99 for all games (Hill et al., 2018). We train PPO agents with $\gamma \in \{0.1, 0.3, 0.5, 0.7, 0.9, 0.9999\}$ and generate saliency maps on the standard image set. The results are shown in Fig. 3. Overall, the RL attention is most similar to human’s when $\gamma = 0.7$ or 0.9 . From the visualizations in Fig. 4 we can see that with small γ s, the agents tend to be myopic and only focus on very few objects. With high γ s, the agents divide their attention into several objects. Since the human gaze model only captures the overt attention and involves typically 1-3 objects, intermediate γ values produce saliency maps that are similar to humans.

For each γ value, we normalize the game score by dividing it by the score obtained by the $\gamma = 0.99$ agent. For most games, this default value has the best performance. However, the performance increases with CCs and negative KL values only up to $\gamma = 0.7$ in Fig. 3. Beyond that, the RL agents need to learn to attend to objects that matter in the long-term, which are likely to be captured by human covert

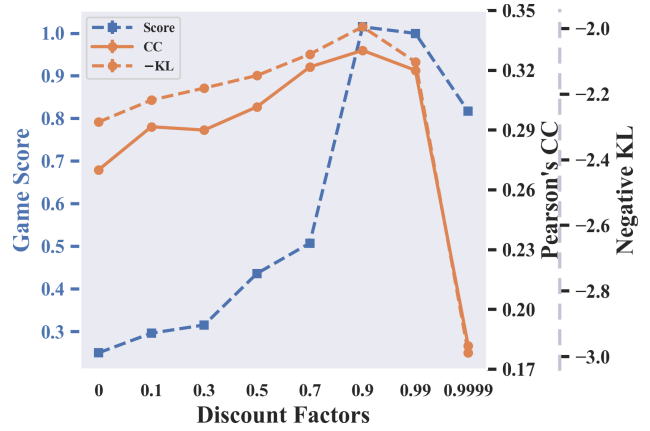


Figure 3. Changes in human and RL attention similarity across different discount factors. Choosing different discount factors affects the RL agent’s attention and performance. The CC, KL, and score results for individual games, as well as more examples, can be found in Appendix 3.

attention and do not show up in our human attention model.

Nonetheless, deviating from the default $\gamma = 0.99$ can lead to better performance. In Seaquest, the agent with $\gamma = 0.9$ achieves 15% higher score than the default agent. Fig. 4b shows that with a lower $\gamma = 0.9$, the agent can focus, like humans, on an immediate threat from the left. Setting $\gamma = 0.99$ or 0.9999 distracts the agent to attend to the oxygen bar at the bottom that is important in the long run but less urgent now. A similar result was found for Ms.Pac-Man with an 18% higher score from the $\gamma = 0.9$ agent than the $\gamma = 0.99$ agent.

This result has an important implication. Atari games are episodic tasks with true $\gamma = 1$ but lower γ values often lead to better performance in practice (Schulman et al., 2017;

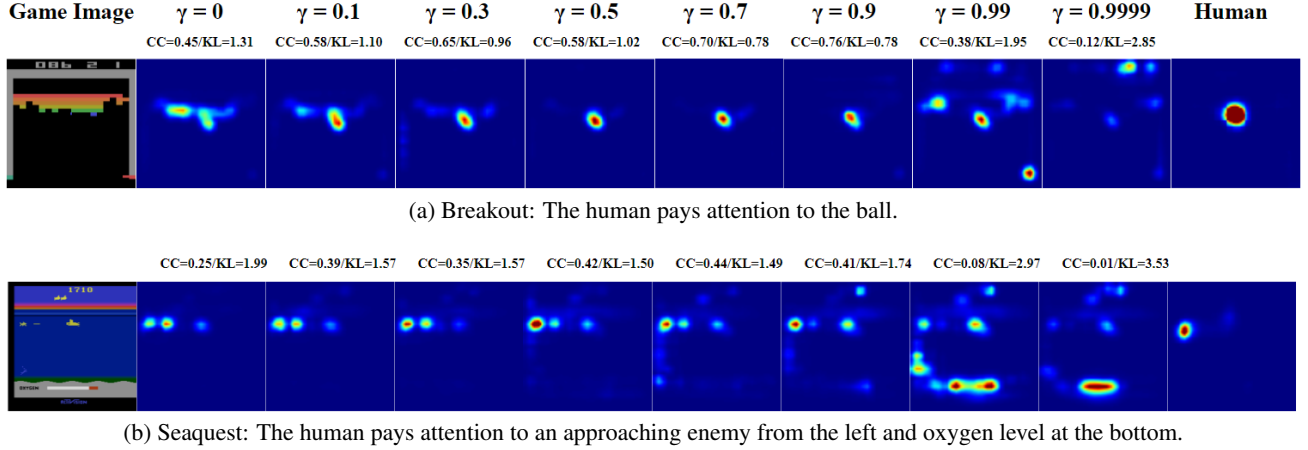


Figure 4. Effect of different discount factors on Ms.Pac-Man and Seaquest agents’ attention. Agents trained with intermediate discount factor values have saliency maps that are more human-like.

Mnih et al., 2015)¹. Fig. 3 shows that $\gamma = 0.9999$ agents perform poorly. We have verified that all $\gamma = 0.9999$ agents (5 random seeds) converged after 200M samples, although to sub-optimal policies (Appendix 3). Again, the reason is that being a little myopic helps the agent focus on the most urgent targets. This result provides another reason, from a perception perspective, for why RL agents need to adjust their planning horizon by reducing the discount factor—confirming the theoretical results provided by Jiang et al. (2015).

4.3. RL versus human attention: Failure states

We now turn to the second research question that concerns explainability in deep RL: Why do deep RL agents make mistakes? Did RL agents fail to attend to the right objects, or did they attend to the right objects but make wrong decisions? We compile a second image set, named failure image set, by recording the game frames right before the RL agent loses a “life” which incurs a large penalty. We locate 100 such instances for each game. Freeway is excluded since the PPO agent learned a policy that is nearly optimal.

Fig. 5 shows two failure cases for Breakout. In the first case, the attention map of the RL agent is extremely different from the human’s, and in the other, they are highly similar. In the first case, the RL agent failed to attend to the ball as the human model did, hence it failed to move the paddle to catch the ball in the next frame (it is still possible to catch that ball). In the second case, both the agent and the human attend to the ball. In this way, we can interpret failure cases

¹Strictly speaking, γ is a property of the MDP, not of the agent. Performance across MDPs with different γ s are not directly comparable in this sense. Varying discount factor and clipping reward are common reward engineering designs that alter the true MDP return to achieve better performance in practice.

using human attention as a reference. If RL attention and human attention are more different in failure than normal states, there is likely to be a perception problem.

Fig. 6 shows the quantitative results for all games. For Montezuma’s Revenge, perception is a problem. The RL attention in failure states becomes less similar to human attention compared to the standard image set, indicated by significantly decreased CC/KL values. Fig. 5 shows that the agent fails to attend to the enemy as the human does.

On the contrary, for Ms. Pac-Man and Seaquest, perception is *not* a major problem. Fig. 6 shows that, in failure states, attention maps of RL agent and human are more similar than in the normal states, suggesting that they generally agree on the objects to be attended to. These are often situations with fewer objects that are more dangerous (see Appendix 4). Hence it is easy for RL agents to attend to the right object but the decision is hard. For example, in Fig. 5 Ms.Pac-Man, the agent attended to the Pac-Man and the enemy ghost similarly to humans. However, the RL agents made the wrong decision and ran into the ghost. For Breakout and Frostbite, the overall differences between failure and normal states are not significant, but one can perform a case-by-case analysis as in Fig. 5.

We conclude that the mistakes made by the RL agents are sometimes related to perceptual errors. Similarity measurements with human attention can help identify and interpret the failures made by RL agents.

4.4. RL versus human attention: Unseen data

Next, we study whether RL agent’s attention generalizes to unseen states. The unseen states are late-game states obtained from human experts’ data (Zhang et al., 2020b) which RL agents have not encountered. We refer to this

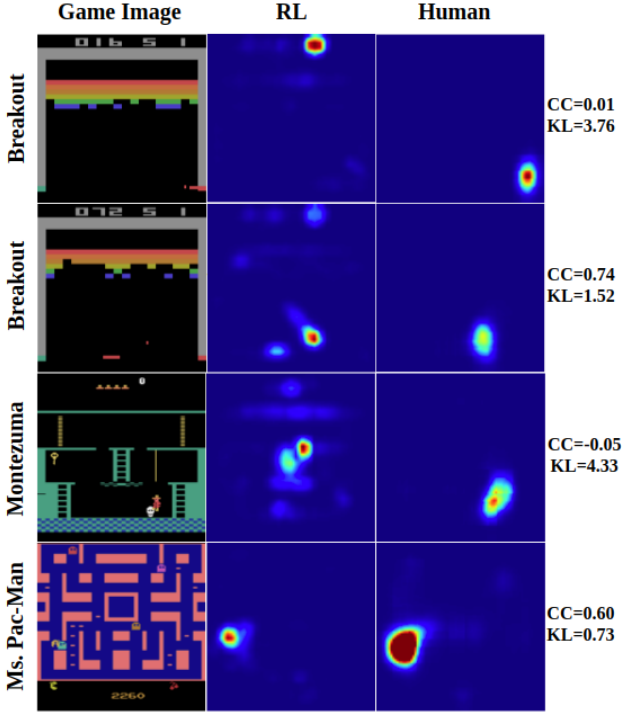


Figure 5. RL vs. human attention in states where RL agents made mistakes. We show examples of RL and human saliency maps for Breakout (top: wrong attention; bottom: right attention but wrong decision), Montezuma’s Revenge (wrong attention), and Ms.Pac-Man (right attention but wrong decision).

set as the unseen image set (100 images per game). Again, Freeway is excluded since the agent is nearly optimal.

Fig. 7b shows the results. For Frostbite and Montezuma’s Revenge, the similarities drop significantly, mostly due to new objects that the agents have never encountered. Fig. 7a shows an example for Montezuma’s Revenge. The agents attended to the ladder, a previously seen object, but failed to attend to a new enemy object on the left like the human did. For Seaquest and Ms. Pac-Man, the RL attention and human attention are more similar on unseen data. This is because there are no new objects in these unseen states – only objects move faster and appear in larger numbers. The player often encounters dangerous states that are close to failure, similar to the ones in Section 4.3. Therefore we observe a similar increase in similarity for Ms.Pac-Man and Seaquest. Breakout is an interesting case. The CC value drops significantly due to unseen spatial layouts of the objects. The KL does not change much because there are no new objects so the agent maintains its attention on the ball and the paddle. More examples are in Appendix 5.

The results suggest that the obstacle to achieving human-level performance for certain games is first a perception challenge – the agents need to learn to recognize, attend



Figure 6. How attention similarities change in failure states compared to normal states. *indicates a significance test result of $p \leq 0.05$; ** indicates $p \leq 0.01$. Error bars are the standard errors of the mean ($n = 100$).

to, and then learn to act upon new objects. This is easy for humans due to their prior knowledge but challenging for RL agents (Lake et al., 2017; Tsividis et al., 2017; Dubey et al., 2018). For the other games, it is a decision-learning problem – the agent’s attention is fairly generalizable and it needs to learn a good policy for challenging states.

4.5. Other Atari agents

The above analyses were done for a particular RL algorithm–PPO. Next we apply our method to other RL algorithms, including C51 (Bellemare et al., 2017), Rainbow (Hessel et al., 2018), DQN (Mnih et al., 2015), and A2C (Mnih et al., 2016), as well as two evolutionary algorithms, GA (Such et al., 2017) and ES (Salimans et al., 2017). We use trained models from Dopamine (Castro et al., 2018) and Atari Model Zoo (Such et al., 2019) in which each algorithm has 3-5 trained models. Fig. 8 shows the result for Ms.Pac-Man. There is a strong positive correlation ($r(22) = 0.927, p < 0.001$) between model performance (in terms of the game score, averaged over 50 episodes each) and similarity measurement (in terms of CC with human attention on the standard image set). The average correlation coefficient for five games is 0.631 (excluding Montezuma since most algorithms have zero scores). The results for individual games can be found in Appendix 6. This result suggests that the positive correlation between model performance and similarity with human attention generalizes to other deep RL algorithms, hence we expect the rest of the analyses we performed with PPO, such as failure diagnosis, can be done for these algorithms as well.

5. Discussion

We provide visual explanations for deep RL agents using human experts’ attention as a reference. We have discussed

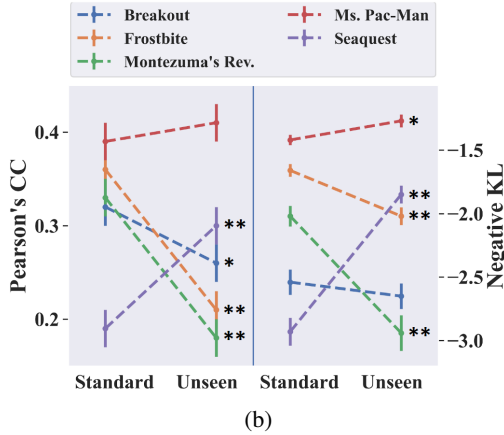
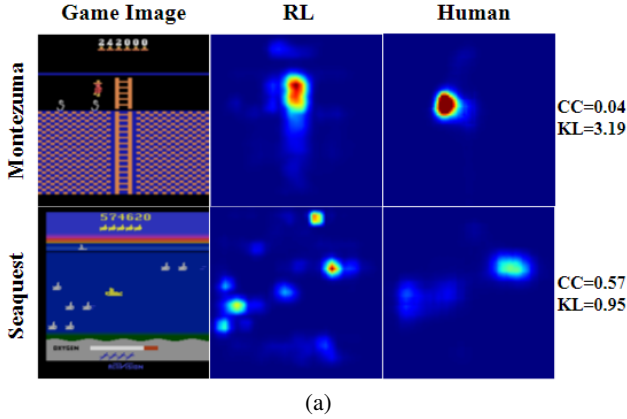


Figure 7. Human versus RL attention in states that RL agents have not seen. (a) Unseen states, for Montezuma’s Revenge (top), the RL agent’s attention is very different from human attention due to a new object on the left. For Seaquest (bottom), they are similar. (b) How attention similarities change in unseen states compared to seen states in different games.

how RL attention develops and becomes more human-like during training, and how varying the discount factor affects learned attention. We show that human attention can be useful in diagnosing an RL agent’s failures. We have also identified further challenges in closing the performance gap between human experts and RL agents. Our analysis is restricted to saliency map comparisons, but other approaches are possible for measuring the similarity of representations learned by different RL agents (Wijmans et al., 2020). Our human attention models, all compiled datasets, and tools for comparing RL attention with human attention is made available for future research in this direction.

For researchers who are interested in RL algorithms, we have gained at least three important insights. First, since the task performance and similarity to human attention are highly correlated, one could use human attention as prior knowledge to guide the learning process of RL agents, e.g., by encouraging them to attend to the correct objects early

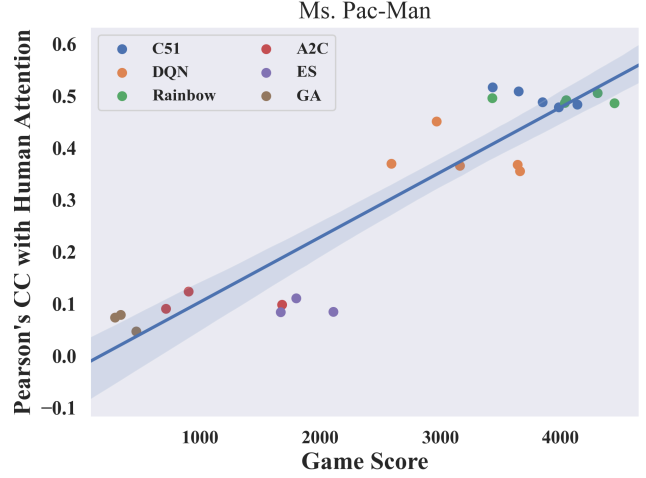


Figure 8. The similarity with human attention is a strong indicator of algorithm’s performance. The line and shaded areas denote the fitted linear regression line and the 95% confidence interval.

in the learning process. This could be especially helpful for games like Seaquest, in which the agent has not learned to focus on the right object after 5120k time steps (Fig. 2). Two human studies using Atari games suggested that prior knowledge, such as perceptual prior, is why humans learn faster and better in these games (Tsividis et al., 2017; Dubey et al., 2018). Then the next question is how to incorporate human attention into DNNs which has been studied in several computer vision tasks (Qiuxia et al., 2020), and has been explored in training deep imitation learning agents (Zhang et al., 2019; Zhang, 2019), deep RL agents (Yuezhong et al., 2018), and deep RL agents with human evaluative feedback (Guan et al., 2020). Our results indicate that RL agents first learn to attend to a few important objects like humans, then learn to attend to other objects. Therefore a desirable loss function would encourage the agents to focus on the regions that the human attended to, but would not penalize the agents for attending to more regions eventually (Saran et al., 2020).

Secondly, our results provide visual explanations for the agents’ performance when varying the discount factors and highlight the importance of choosing proper planning horizons with appropriate discount factors. Recent works confirm this by showing that it is beneficial to have an adaptive discount factor (Badia et al., 2020) or multiple discount factors (Fedus et al., 2019).

At last, failure analysis could identify states where agent’s attention drastically differs from expert humans. These are the states that may need human intervention/correction in a human-in-the-loop RL paradigm. By publishing our human gaze prediction model researchers can diagnose their algorithms with the states of their interest.

For researchers who are interested in using RL as models

for cognition, it is perhaps both surprising and encouraging to see that RL agents trained from scratch with only images and reward signals can develop attention maps that are similar to humans, especially when considering that they have very little prior knowledge. This result is similar to previous research that shows CNNs trained from image classification tasks can learn features that are similar to the ones in the visual cortex (Eickenberg et al., 2017; Yamins et al., 2013; 2014). Consistent with previous findings, we show that model task performance and feature similarity are highly correlated (Yamins et al., 2014). Our results are complementary to the recent findings using human fMRI data when playing Atari games (Cross et al., 2020), suggesting that deep RLs can learn biologically plausible representations and can be used as models for human gaze, decision, and brain activities.

Multiple factors are important for interpreting our results and could explain the remaining differences between human attention and RL attention. The first one is the overt vs. covert attention issue discussed earlier. Humans store information in memory and do not need to constantly move their eyes to attend to all task-relevant objects. To complete the human attention map, in addition to gaze data, one will need to retrieve human covert attention from brain activity data, a technique that became possible recently (Leong et al., 2017; Cross et al., 2020). Another factor is human intrinsic reward. Humans are likely to have internal reward functions that are different from the ones provided by the game environment, and reward is known to affect attention (Rothkopf et al., 2007; Leong et al., 2017).

A closely related research direction compares a human player’s *policy* with an RL agent’s learned policy (Moore & Stamper, 2019) which could further allow us to better understand the similarities and differences between humans and RL agents. However, as we have shown here, the difference in decisions could be due to perception, which needs to be considered while comparing policies. Our approach lays the groundwork for future research in this direction.

References

- Alharin, A., Doan, T.-N., and Sartipi, M. Reinforcement learning interpretation methods: A survey. *IEEE Access*, 8:171058–171077, 2020.
- Badia, A. P., Piot, B., Kapturowski, S., Sprechmann, P., Vitvitskyi, A., Guo, Z. D., and Blundell, C. Agent57: Outperforming the atari human benchmark. In *International Conference on Machine Learning*, pp. 507–517. PMLR, 2020.
- Bellemare, M. G., Naddaf, Y., Veness, J., and Bowling, M. The arcade learning environment: An evaluation platform for general agents. *Journal of Artificial Intelligence Research*, 47:253–279, 2013.
- Bellemare, M. G., Dabney, W., and Munos, R. A distributional perspective on reinforcement learning. In *International Conference on Machine Learning*, pp. 449–458. PMLR, 2017.
- Borji, A. and Itti, L. Defending yarbus: Eye movements reveal observers’ task. *Journal of Vision*, 14(3):29–29, 2014.
- Borji, A., Cheng, M.-M., Jiang, H., and Li, J. Salient object detection: A benchmark. *IEEE Transactions on Image Processing*, 24(12):5706–5722, 2015.
- Bylinskii, Z., Recasens, A., Borji, A., Oliva, A., Torralba, A., and Durand, F. Where should saliency models look next? In *European Conference on Computer Vision (ECCV)*, pp. 809–824. Springer, 2016.
- Bylinskii, Z., Judd, T., Oliva, A., Torralba, A., and Durand, F. What do different evaluation metrics tell us about saliency models? *IEEE Transactions on Pattern Analysis and Machine Intelligence*, 41(3):740–757, 2019.
- Castro, P. S., Moitra, S., Gelada, C., Kumar, S., and Bellemare, M. G. Dopamine: A Research Framework for Deep Reinforcement Learning. 2018. URL <http://arxiv.org/abs/1812.06110>.
- Chattopadhyay, A., Sarkar, A., Howlader, P., and Balasubramanian, V. N. Grad-cam++: Generalized gradient-based visual explanations for deep convolutional networks. In *2018 IEEE Winter Conference on Applications of Computer Vision (WACV)*, pp. 839–847. IEEE, 2018.
- Cross, L., Cockburn, J., Yue, Y., and O’Doherty, J. P. Using deep reinforcement learning to reveal how the brain encodes abstract state-space representations in high-dimensional environments. *Neuron*, 2020.
- Dabkowski, P. and Gal, Y. Real time image saliency for black box classifiers. In *Advances in Neural Information Processing Systems*, pp. 6967–6976, 2017.
- Das, A., Agrawal, H., Zitnick, L., Parikh, D., and Batra, D. Human attention in visual question answering: Do humans and deep networks look at the same regions? *Computer Vision and Image Understanding*, 163:90–100, 2017.
- Deng, T., Yan, H., Qin, L., Ngo, T., and Manjunath, B. How do drivers allocate their potential attention? driving fixation prediction via convolutional neural networks. *IEEE Transactions on Intelligent Transportation Systems*, 2019.

- Diaz, G., Cooper, J., Rothkopf, C., and Hayhoe, M. Sacca-
cades to future ball location reveal memory-based pre-
diction in a virtual-reality interception task. *Journal of*
Vision, 13(1):20–20, 2013.
- Dubey, R., Agrawal, P., Pathak, D., Griffiths, T. L., and
Efros, A. A. Investigating human priors for playing video
games. *arXiv preprint arXiv:1802.10217*, 2018.
- Eickenberg, M., Gramfort, A., Varoquaux, G., and Thirion,
B. Seeing it all: Convolutional network layers map the
function of the human visual system. *NeuroImage*, 152:
184–194, 2017.
- Farnebäck, G. Two-frame motion estimation based on poly-
nomial expansion. *Image analysis*, pp. 363–370, 2003.
- Fedus, W., Gelada, C., Bengio, Y., Bellemare, M. G., and
Larochelle, H. Hyperbolic discounting and learning over
multiple horizons. *arXiv preprint arXiv:1902.06865*,
2019.
- Fong, R. C. and Vedaldi, A. Interpretable explanations of
black boxes by meaningful perturbation. In *Proceed-
ings of the IEEE International Conference on Computer*
Vision, pp. 3429–3437, 2017.
- Greydanus, S., Koul, A., Dodge, J., and Fern, A. Visual-
izing and understanding atari agents. In *International*
Conference on Machine Learning, pp. 1792–1801, 2018.
- Grimm, C., Arumugam, D., Karamcheti, S., Abel, D., Wong,
L. L., and Littman, M. L. Modeling latent attention within
neural networks. *arXiv preprint arXiv:1706.00536*, 2017.
- Guan, L., Verma, M., Guo, S., Zhang, R., and Kambhampati,
S. Explanation augmented feedback in human-in-the-loop
reinforcement learning, 2020.
- Gupta, P., Puri, N., Verma, S., Singh, S., Kayastha, D.,
Deshmukh, S., and Krishnamurthy, B. Explain your
move: Understanding agent actions using focused feature
saliency. *arXiv preprint arXiv:1912.12191*, 2019.
- He, S., Tavakoli, H. R., Borji, A., Mi, Y., and Pugeault, N.
Understanding and visualizing deep visual saliency mod-
els. In *Proceedings of the IEEE Conference on Computer*
Vision and Pattern Recognition, pp. 10206–10215, 2019a.
- He, S., Tavakoli, H. R., Borji, A., and Pugeault, N. Human
attention in image captioning: Dataset and analysis. In
Proceedings of the IEEE International Conference on
Computer Vision, pp. 8529–8538, 2019b.
- Hessel, M., Modayil, J., Van Hasselt, H., Schaul, T., Ostro-
vski, G., Dabney, W., Horgan, D., Piot, B., Azar, M., and
Silver, D. Rainbow: Combining improvements in deep re-
inforcement learning. In *Thirty-Second AAAI Conference*
on Artificial Intelligence, 2018.
- Heuillet, A., Couthouis, F., and Díaz-Rodríguez, N. Explain-
ability in deep reinforcement learning. *Knowledge-Based*
Systems, pp. 106685, 2020.
- Hill, A., Raffin, A., Ernestus, M., Gleave, A., Kanervisto, A.,
Traore, R., Dhariwal, P., Hesse, C., Klimov, O., Nichol,
A., Plappert, M., Radford, A., Schulman, J., Sidor, S.,
and Wu, Y. Stable baselines. [https://github.com/
hill-a/stable-baselines](https://github.com/hill-a/stable-baselines), 2018.
- Huber, T., Limmer, B., and André, E. Benchmark-
ing perturbation-based saliency maps for explaining
deep reinforcement learning agents. *arXiv preprint*
arXiv:2101.07312, 2021.
- Huth, A. G., De Heer, W. A., Griffiths, T. L., Theunissen,
F. E., and Gallant, J. L. Natural speech reveals the se-
mantic maps that tile human cerebral cortex. *Nature*, 532
(7600):453–458, 2016.
- Itti, L., Koch, C., and Niebur, E. A model of saliency-
based visual attention for rapid scene analysis. *IEEE*
Transactions on Pattern Analysis & Machine Intelligence,
(11):1254–1259, 1998.
- Iyer, R., Li, Y., Li, H., Lewis, M., Sundar, R., and Sycara,
K. Transparency and explanation in deep reinforcement
learning neural networks. In *Proceedings of the 2018*
AAAI/ACM Conference on AI, Ethics, and Society, pp.
144–150, 2018.
- Jain, S. and Huth, A. Incorporating context into language
encoding models for fmri. In *Advances in Neural Infor-
mation Processing Systems*, pp. 6628–6637, 2018.
- Jaunet, T., Vuillemot, R., and Wolf, C. Drlviz: Understand-
ing decisions and memory in deep reinforcement learning.
arXiv preprint arXiv:1909.02982, 2019.
- Jiang, N., Kulesza, A., Singh, S., and Lewis, R. The depen-
dence of effective planning horizon on model accuracy.
In *Proceedings of the 2015 International Conference on*
Autonomous Agents and Multiagent Systems, pp. 1181–
1189, 2015.
- Joo, H.-T. and Kim, K.-J. Visualization of deep reinforce-
ment learning using grad-cam: How ai plays atari games?
In *2019 IEEE Conference on Games (CoG)*, pp. 1–2.
IEEE, 2019.
- Lai, Q., Wang, W., Khan, S., Shen, J., Sun, H., and Shao, L.
Human\textit {vs} machine attention in neural networks:
A comparative study. *arXiv preprint arXiv:1906.08764*,
2019.
- Lake, B. M., Ullman, T. D., Tenenbaum, J. B., and Gersh-
man, S. J. Building machines that learn and think like
people. *Behavioral and Brain Sciences*, 40, 2017.

- Le Meur, O. and Baccino, T. Methods for comparing scan-paths and saliency maps: strengths and weaknesses. *Behavior research methods*, 45(1):251–266, 2013.
- Leong, Y. C., Radulescu, A., Daniel, R., DeWoskin, V., and Niv, Y. Dynamic interaction between reinforcement learning and attention in multidimensional environments. *Neuron*, 93(2):451–463, 2017.
- Li, Y., Liu, M., and Rehg, J. M. In the eye of beholder: Joint learning of gaze and actions in first person video. In *European Conference on Computer Vision (ECCV)*, pp. 619–635, 2018.
- Mahendran, A. and Vedaldi, A. Visualizing deep convolutional neural networks using natural pre-images. *International Journal of Computer Vision*, 120(3):233–255, 2016.
- Merel, J., Aldarondo, D., Marshall, J., Tassa, Y., Wayne, G., and Ölveczky, B. Deep neuroethology of a virtual rodent. *arXiv preprint arXiv:1911.09451*, 2019.
- Mnih, V., Kavukcuoglu, K., Silver, D., Rusu, A. A., Veness, J., Bellemare, M. G., Graves, A., Riedmiller, M., Fidjeland, A. K., Ostrovski, G., et al. Human-level control through deep reinforcement learning. *Nature*, 518(7540): 529–533, 2015.
- Mnih, V., Badia, A. P., Mirza, M., Graves, A., Lillicrap, T., Harley, T., Silver, D., and Kavukcuoglu, K. Asynchronous methods for deep reinforcement learning. In *International conference on machine learning*, pp. 1928–1937, 2016.
- Moore, S. and Stamper, J. C. Exploring expertise through visualizing agent policies and human strategies in open-ended games. In *EDM (Workshops)*, pp. 30–37, 2019.
- Mott, A., Zoran, D., Chrzanowski, M., Wierstra, D., and Rezende, D. J. Towards interpretable reinforcement learning using attention augmented agents. In *Advances in Neural Information Processing Systems*, pp. 12329–12338, 2019.
- Mousavi, S., Schukat, M., Howley, E., Borji, A., and Moza-yani, N. Learning to predict where to look in interactive environments using deep recurrent q-learning. *arXiv preprint arXiv:1612.05753*, 2016.
- Muddamsetty, S. M., Jahromi, M. N., Ciontos, A. E., Fenoy, L. M., and Moeslund, T. B. Introducing and assessing the explainable ai (xai) method: Sidu. *arXiv preprint arXiv:2101.10710*, 2021.
- Nguyen, T. V., Zhao, Q., and Yan, S. Attentive systems: A survey. *International Journal of Computer Vision*, 126 (1):86–110, 2018.
- Nikulin, D., Ianina, A., Aliev, V., and Nikolenko, S. Free-lunch saliency via attention in atari agents. *arXiv preprint arXiv:1908.02511*, 2019.
- Palazzi, A., Abati, D., Calderara, S., Solera, F., and Cucchiara, R. Predicting the driver’s focus of attention: the dr (eye) ve project. *IEEE Transactions on Pattern Analysis and Machine Intelligence*, 2018.
- Posner, M. I. Orienting of attention. *Quarterly Journal of Experimental Psychology*, 32(1):3–25, 1980.
- Puiutta, E. and Veith, E. M. Explainable reinforcement learning: A survey. In *International Cross-Domain Conference for Machine Learning and Knowledge Extraction*, pp. 77–95. Springer, 2020.
- Puri, N., Verma, S., Gupta, P., Kayastha, D., Deshmukh, S., Krishnamurthy, B., and Singh, S. Explain your move: Understanding agent actions using specific and relevant feature attribution. In *International Conference on Learning Representations*, 2019.
- Qiuxia, L., Khan, S., Nie, Y., Hanqiu, S., Shen, J., and Shao, L. Understanding more about human and machine attention in deep neural networks. *IEEE Transactions on Multimedia*, 2020.
- Ribeiro, M. T., Singh, S., and Guestrin, C. ” why should i trust you?” explaining the predictions of any classifier. In *Proceedings of the 22nd ACM SIGKDD International Conference on Knowledge Discovery and Data Mining*, pp. 1135–1144, 2016.
- Robinson, D. The mechanics of human saccadic eye movement. *The Journal of physiology*, 174(2):245–264, 1964.
- Rothkopf, C. A., Ballard, D. H., and Hayhoe, M. M. Task and context determine where you look. *Journal of Vision*, 7(14):16–16, 2007.
- Salimans, T., Ho, J., Chen, X., Sidor, S., and Sutskever, I. Evolution strategies as a scalable alternative to reinforcement learning. *arXiv preprint arXiv:1703.03864*, 2017.
- Saran, A., Zhang, R., Short, E. S., and Niekum, S. Efficiently guiding imitation learning algorithms with human gaze. *arXiv preprint arXiv:2002.12500*, 2020.
- Schulman, J., Wolski, F., Dhariwal, P., Radford, A., and Klimov, O. Proximal policy optimization algorithms. *arXiv preprint arXiv:1707.06347*, 2017.
- Selvaraju, R. R., Cogswell, M., Das, A., Vedantam, R., Parikh, D., and Batra, D. Grad-cam: Visual explanations from deep networks via gradient-based localization. In *Proceedings of the IEEE International Conference on Computer Vision*, pp. 618–626, 2017.

- Shi, W., Wang, Z., Song, S., and Huang, G. Self-supervised discovering of causal features: Towards interpretable reinforcement learning. *arXiv preprint arXiv:2003.07069*, 2020.
- Shrikumar, A., Greenside, P., and Kundaje, A. Learning important features through propagating activation differences. In *Proceedings of the 34th International Conference on Machine Learning-Volume 70*, pp. 3145–3153. JMLR. org, 2017.
- Simonyan, K., Vedaldi, A., and Zisserman, A. Deep inside convolutional networks: Visualising image classification models and saliency maps. *arXiv preprint arXiv:1312.6034*, 2013.
- Springenberg, J. T., Dosovitskiy, A., Brox, T., and Riedmiller, M. Striving for simplicity: The all convolutional net. *arXiv preprint arXiv:1412.6806*, 2014.
- Such, F. P., Madhavan, V., Conti, E., Lehman, J., Stanley, K. O., and Clune, J. Deep neuroevolution: Genetic algorithms are a competitive alternative for training deep neural networks for reinforcement learning. *arXiv preprint arXiv:1712.06567*, 2017.
- Such, F. P., Madhavan, V., Liu, R., Wang, R., Castro, P. S., Li, Y., Zhi, J., Schubert, L., Bellemare, M. G., Clune, J., et al. An atari model zoo for analyzing, visualizing, and comparing deep reinforcement learning agents. In *Proceedings of the 28th International Joint Conference on Artificial Intelligence*, pp. 3260–3267. AAAI Press, 2019.
- Sundararajan, M., Taly, A., and Yan, Q. Axiomatic attribution for deep networks. In *Proceedings of the 34th International Conference on Machine Learning-Volume 70*, pp. 3319–3328. JMLR. org, 2017.
- Tavakoli, H. R., Shetty, R., Borji, A., and Laaksonen, J. Paying attention to descriptions generated by image captioning models. In *Proceedings of the IEEE International Conference on Computer Vision*, pp. 2487–2496, 2017.
- Tsividis, P. A., Pouncy, T., Xu, J. L., Tenenbaum, J. B., and Gershman, S. J. Human learning in atari. 2017.
- Wang, J., Gou, L., Shen, H.-W., and Yang, H. Dqnviz: A visual analytics approach to understand deep q-networks. *IEEE Transactions on Visualization and Computer Graphics*, 25(1):288–298, 2018.
- Weitkamp, L., van der Pol, E., and Akata, Z. Visual rationalizations in deep reinforcement learning for atari games. In *Benelux Conference on Artificial Intelligence*, pp. 151–165. Springer, 2018.
- Wijmans, E., Straub, J., Batra, D., Essa, I., Hoffman, J., and Morcos, A. Analyzing visual representations in embodied navigation tasks. *arXiv preprint arXiv:2003.05993*, 2020.
- Yamins, D. L., Hong, H., Cadieu, C., and DiCarlo, J. J. Hierarchical modular optimization of convolutional networks achieves representations similar to macaque it and human ventral stream. In *Advances in Neural Information Processing Systems*, pp. 3093–3101, 2013.
- Yamins, D. L., Hong, H., Cadieu, C. F., Solomon, E. A., Seibert, D., and DiCarlo, J. J. Performance-optimized hierarchical models predict neural responses in higher visual cortex. *Proceedings of the National Academy of Sciences*, 111(23):8619–8624, 2014.
- Yang, Z., Bai, S., Zhang, L., and Torr, P. H. Learn to interpret atari agents. *arXiv preprint arXiv:1812.11276*, 2018.
- Yuezhong, L., Zhang, R., and Ballard, D. H. An initial attempt of combining visual selective attention with deep reinforcement learning. *arXiv preprint arXiv:1811.04407*, 2018.
- Zeiler, M. D. Adadelta: an adaptive learning rate method. *arXiv preprint arXiv:1212.5701*, 2012.
- Zeiler, M. D. and Fergus, R. Visualizing and understanding convolutional networks. In *European Conference on Computer Vision (ECCV)*, pp. 818–833. Springer, 2014.
- Zhang, J., Bargal, S. A., Lin, Z., Brandt, J., Shen, X., and Sclaroff, S. Top-down neural attention by excitation backprop. *International Journal of Computer Vision*, 126(10):1084–1102, 2018a.
- Zhang, R. Attention guided imitation learning and reinforcement learning. In *Proceedings of the AAAI Conference on Artificial Intelligence*, volume 33, pp. 9906–9907, 2019.
- Zhang, R., Liu, Z., Zhang, L., Whritner, J. A., Muller, K. S., Hayhoe, M. M., and Ballard, D. H. Agil: Learning attention from human for visuomotor tasks. In *European Conference on Computer Vision (ECCV)*, pp. 692–707. Springer, 2018b.
- Zhang, R., Torabi, F., Guan, L., Ballard, D. H., and Stone, P. Leveraging human guidance for deep reinforcement learning tasks. In *Proceedings of the 28th International Joint Conference on Artificial Intelligence*, pp. 6339–6346. AAAI Press, 2019.
- Zhang, R., Saran, A., Liu, B., Zhu, Y., Guo, S., Niekum, S., Ballard, D., and Hayhoe, M. Human gaze assisted artificial intelligence: A review. In *IJCAI: proceedings of the conference*, volume 2020, pp. 4951. NIH Public Access, 2020a.

Zhang, R., Walshe, C., Liu, Z., Guan, L., Muller, K. S., Whritner, J. A., Zhang, L., Hayhoe, M. M., and Ballard, D. H. Atari-head: Atari human eye-tracking and demonstration dataset. In *Thirty-Fourth AAAI Conference on Artificial Intelligence*. AAAI Press, 2020b.

Zhou, B., Khosla, A., Lapedriza, A., Oliva, A., and Torralba, A. Learning deep features for discriminative localization. In *Proceedings of the IEEE Conference on Computer Vision and Pattern Recognition*, pp. 2921–2929, 2016.

Zintgraf, L. M., Cohen, T. S., Adel, T., and Welling, M. Visualizing deep neural network decisions: Prediction difference analysis. *arXiv preprint arXiv:1702.04595*, 2017.

Zuo, Z., Yang, L., Peng, Y., Chao, F., and Qu, Y. Gaze-informed egocentric action recognition for memory aid systems. *IEEE Access*, 6:12894–12904, 2018.

Appendix 1: Human Attention Model and Attention Prediction Video

In order to get human saliency maps for the data generated by reinforcement learning (RL) agents, we need a model that can predict human attention. We have found that the accuracy of such a model is critical for making attention comparison meaningful. Here we discuss details for implementing human attention models. The data we use is from Atari-HEAD dataset (Zhang et al., 2020b)²The trained models and network architecture will be made available online. The prediction results for each individual game is shown in Table 1. For readers to get an intuitive sense of how accurate the prediction results are, we have included a gaze prediction video for all 6 games in the multimedia appendix.

- **Input image preprocessing:** The images are reshaped from 160×210 to 84×84 with bilinear interpolation and converted into grayscale. Then we scale the pixel values to be in the range of $[0, 1]$ by dividing them by 255. So the inputs are consistent with the inputs to the reinforcement learning agents.
- **Human gaze label preprocessing:** Following the convention, we convert discrete gaze positions into continuous distribution by blurring each gaze location using a 2D Gaussian with σ that is equivalent to one visual degree (Le Meur & Baccino, 2013; Zhang et al., 2020b).
- **Model architecture:** The human gaze prediction model is adapted from (Zhang et al., 2020b). The network has three convolution layers followed by three deconvolution layers. Their parameters are as follows:
 - Convolution layer 1: 32 filters, kernel size = 8×8 , stride = 4, followed by relu activation, batch normalization, and dropout.
 - Convolution layer 2: 64 filters, kernel size = 4×4 , stride = 2, followed by relu activation, batch normalization, and dropout.
 - Convolution layer 3: 64 filters, kernel size = 3×3 , stride = 1, followed by relu activation, batch normalization, and dropout.
 - Deconvolution layer 1: 64 filters, kernel size = 3×3 , stride = 1, followed by relu activation, batch normalization, and dropout.
 - Deconvolution layer 2: 64 filters, kernel size = 4×4 , stride = 2, followed by relu activation, batch normalization, and dropout.
 - Deconvolution layer 3: 1 filter, kernel size = 8×8 , stride = 4, followed by a softmax layer.

The network is implemented using Tensorflow 1.8.0 and Keras 2.1.5. The same deep network architecture and hyperparameters are used for all games.

- **Optimizer:** The optimizer is Adadelata which is a method with adaptive learning rate (Zeiler, 2012). We use learning rate = 1.0, decay rate $\rho = 0.95$, and $\epsilon = 1e - 8$.
- **Data:** For each game, we use approximately 80% gaze data (16 trials) for training and 20% (4 trials) for testing. For this dataset, two adjacent images or gaze positions are highly correlated. We avoid putting one frame in the training set and its neighboring frame in the testing set by using complete trials as the testing set.
- **Hardware:** Training was conducted on server clusters with NVIDIA GTX 1080 and 1080Ti GPUs.

Appendix 2: The Effects of Learning on Attention

In Appendix 2 to 5, we will show statistics and example images of each game. Atari games have very different reward mechanisms, visual features, and dynamics. Hence, it is often difficult to find an RL algorithm that works best for all games. We hope that, by showing results for individual games, researchers will gain insights into why a particular algorithm (like PPO here) performs well or poorly for a particular game.

In Figure 1 to 6 we show how the attention of the RL agent (PPO) evolves over time compared to human attention. Part (a) of each figure shows the similarity metrics: Pearson’s Correlation Coefficient (CC) and negative Kullback-Leibler Divergence (KL) values over training time steps. The values are averaged over 100 images in the standard image set (as described in section 3.3). (a) also shows the game scores (averaged over 50 episodes) over training time steps. Part (b) of each figure shows an example game image. It also includes the average saliency maps of the RL agents during training and a human saliency map predicted by the human model for the selected game image. Note that KL values are negated for better visualization.

Appendix 3: The Effects of Discount Factors on Attention

Similar to Appendix 2, Figure 7 to 12 shows how the attention of the RL agent (PPO) changes when we vary the discount factor, compared to human attention. $\gamma = 0.99$ is the default value for most RL algorithms (Hill et al., 2018; Schulman et al., 2017). Each Figure (a) shows the similarity metrics: CC and negative KL values over different discount

²Available for download at: <https://zenodo.org/record/3451402>

	Breakout	Freeway	Frostbite	Ms.Pac-Man	Montezuma	Seaquest
AUC	0.973	0.977	0.962	0.984	0.947	0.964
CC	0.575	0.627	0.515	0.666	0.447	0.546
KL	1.302	1.205	1.555	1.027	1.882	1.495

Table 1. Human gaze prediction accuracy for 6 Atari games. Random prediction baseline: AUC = 0.500, KL = 6.100, CC = 0.000. The prediction accuracy is comparable to previous results (Zhang et al., 2020b) and is considered high according to the visual saliency research standards (Bylinskii et al., 2019). A gaze prediction video for all 6 games has been included in the multimedia appendix.

factors. The values are averaged over 100 images in the standard image set. (a) also shows the game scores (averaged over 50 episodes) over discount factors. Each Figure (b) shows an example game image, RL agents’ saliency maps with different discount factors γ , and human saliency map predicted by the human model. Note that KL values are negated for better visualization.

based and value-based algorithms, we ignore attention that is on game scores when doing comparisons (by cropping out that part of the image when calculating the similarity), following the standard approach (Greydanus et al., 2018; Gupta et al., 2019; Huber et al., 2021).

Appendix 4: Failure States Analysis

Figures 13 and 14 show RL agents’ saliency maps compared to human’s in failure states. These states are game frames right before the RL agent loses a “life” which incurs a large penalty in Atari games. This analysis is helpful in answering the question: Did RL agents make mistakes because they fail to attend to the right objects, or did they attend to the right objects but make wrong decisions? Figure 13 shows the games that belong to the former case, and Figure 14 shows the games that belong to the latter case. Freeway is excluded here since the PPO agent learned a policy that is nearly optimal.

Appendix 5: Generalizing to Unseen Data

Figure 15 to 16 show RL agents’ saliency maps compared to human’s in unseen states. The unseen states are end-game states obtained from human experts’ data which RL agents have not encountered during learning. The goal is to see whether RL agents’ attention can reasonably generalize to these unseen states. Again, Freeway is excluded here since the PPO agent learned a policy that is nearly optimal.

Appendix 6: Other Deep RL Algorithms

There is a positive correlation between model performance (in terms of the game score, averaged over 50 episodes each) and similarity (in terms of CC on the standard image set) with human attention. Fig. 17 shows the result for Breakout, Freeway, Frostbite, and Seaquest (Ms.Pac-Man’s result is in the main text). Montezuma’s Revenge is excluded because most algorithms have a score of zero. Note algorithms such as DQN outputs state-action values instead of policy hence they will attend to game scores at the top or the bottom of the screen. In order to ensure a fair comparison for policy-

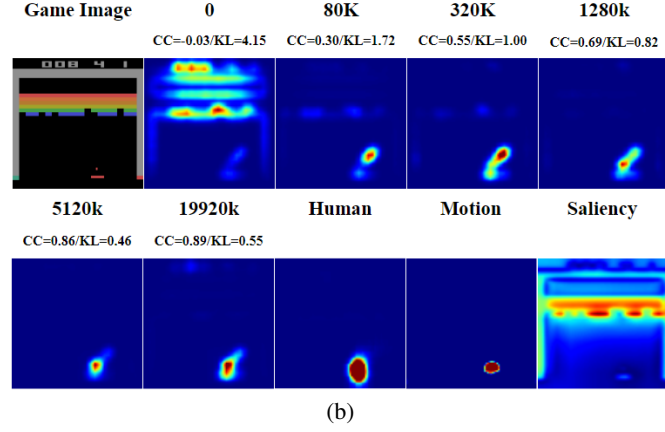
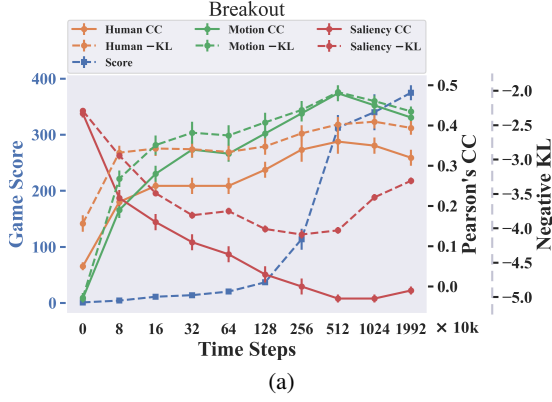


Figure 1. Breakout: (a) Human and RL saliency maps become more similar over training time steps. Pearson's correlation coefficients between game score and human are CC: $r(8) = 0.664, p < 0.05$, KL: $r(8) = 0.622, p = 0.054$; between game score and motion are CC: $r(8) = 0.641, p < 0.05$, KL: $r(8) = 0.550, p = 0.100$; between game score and saliency are CC: $r(8) = -0.661, p < 0.05$, KL: $r(8) = -0.215, p = 0.551$. (b) The RL agents gradually learn to focus their attention on both the paddle and the ball as humans do.

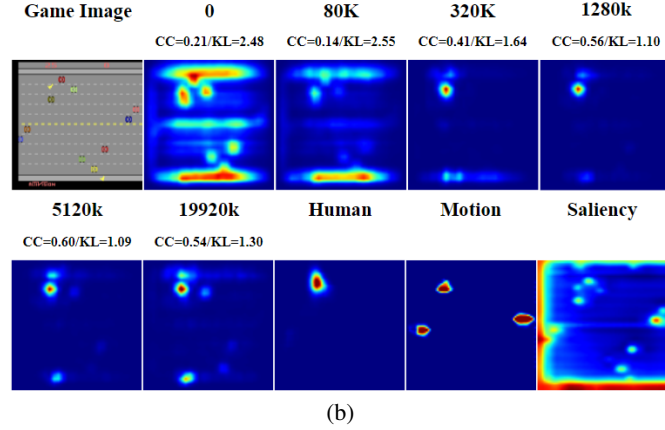
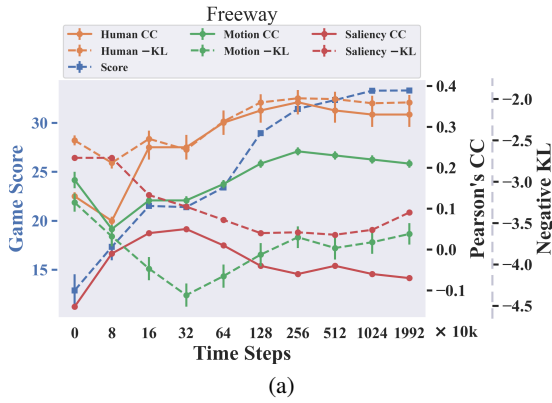


Figure 2. Freeway: (a) Human and RL saliency maps become more similar over training time steps. Pearson's correlation coefficients between game score and human are CC: $r(8) = 0.878, p < 0.001$, KL: $r(8) = 0.888, p < 0.001$; between game score and motion are CC: $r(8) = 0.765, p < 0.01$, KL: $r(8) = 0.080, p = 0.826$; between game score and saliency are CC: $r(8) = -0.078, p = 0.830$, KL: $r(8) = -0.878, p < 0.001$. (b) The RL agents gradually learn to focus their attention on the yellow chicken being controlled to cross the highway. The similarity values decrease a little at the end of the training because the RL agents also learn to attend to the starting point at the bottom of the image.

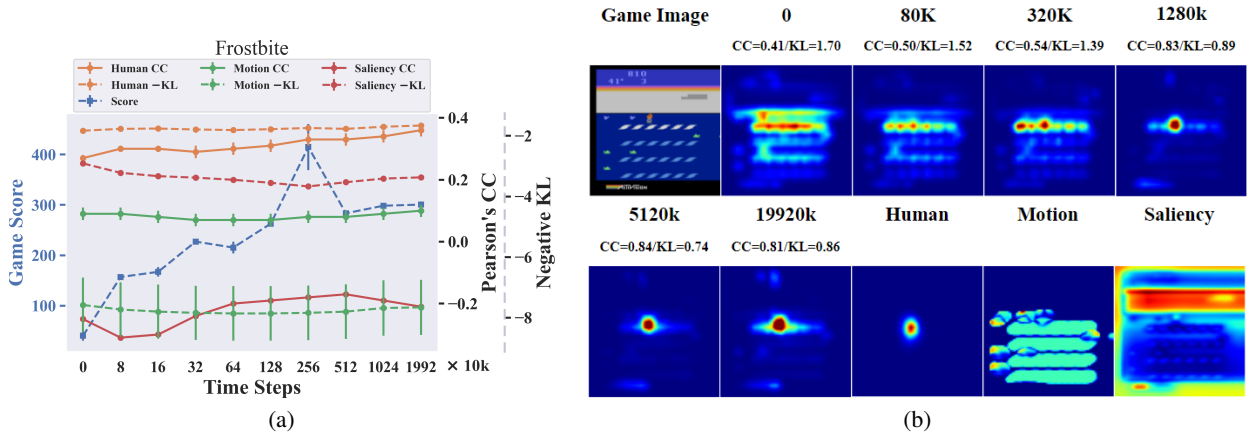


Figure 3. Frostbite: (a) Human and RL saliency maps become more similar over training time steps. Pearson’s correlation coefficients between game score and human are CC: $r(8) = 0.791, p < 0.01$, KL: $r(8) = 0.620, p = 0.056$; between game score and motion are CC: $r(8) = -0.087, p = 0.811$, KL: $r(8) = -0.443, p = 0.200$; between game score and saliency are CC: $r(8) = 0.688, p < 0.05$, KL: $r(8) = -0.900, p < 0.001$. (b) The RL agents gradually learn to attend to the little person being controlled in the middle like humans do.

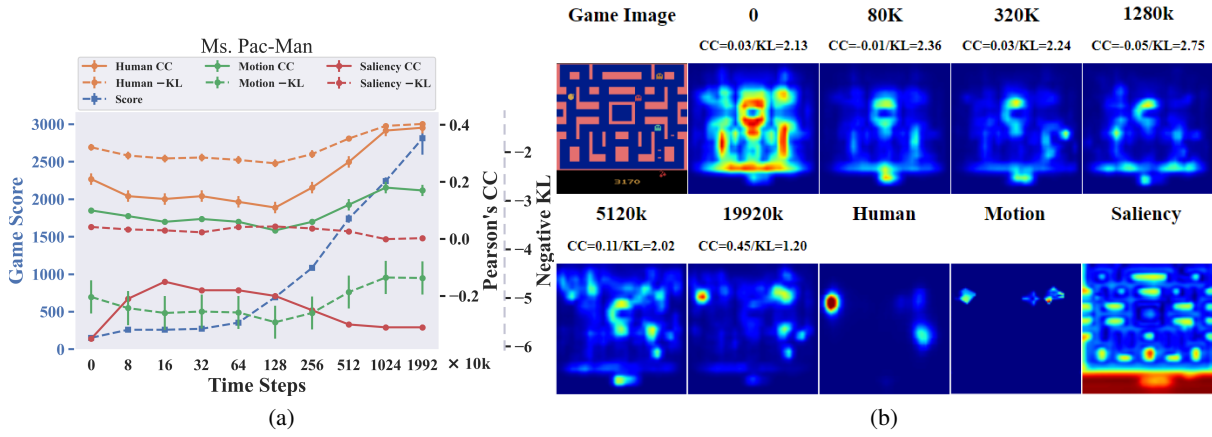


Figure 4. Ms. Pac-Man: (a) Human and RL saliency maps become less similar at first, and then become more similar during training. Pearson’s correlation coefficients between game score and human are CC: $r(8) = 0.910, p < 0.001$, KL: $r(8) = 0.893, p < 0.001$; between game score and motion are CC: $r(8) = 0.819, p < 0.01$, KL: $r(8) = 0.809, p < 0.01$; between game score and saliency are CC: $r(8) = -0.586, p = 0.075$, KL: $r(8) = -0.806, p < 0.01$. (b) The RL agents eventually learn to attend to the Pac-Man on the left and an enemy ghost on the right like humans do.

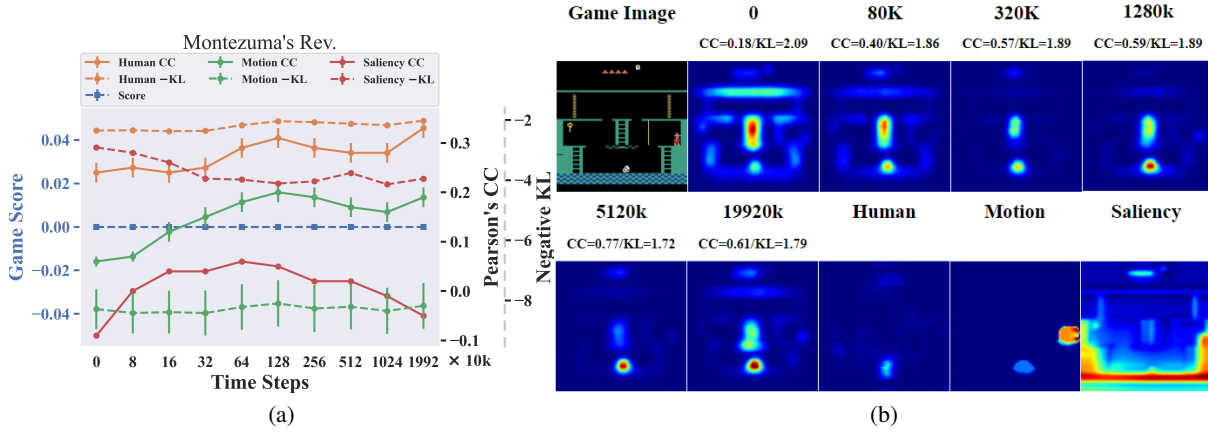


Figure 5. Montezuma's Revenge: (a) Human and RL saliency maps becomes more similar over training time steps. Note that this is a difficult game for RL agents and they never learn to score. Pearson's correlation coefficients are undefined in this case. (b) The RL agents learn to attend to the enemy at the bottom like humans do, but they are uncertain about the importance of the ladder in the middle.

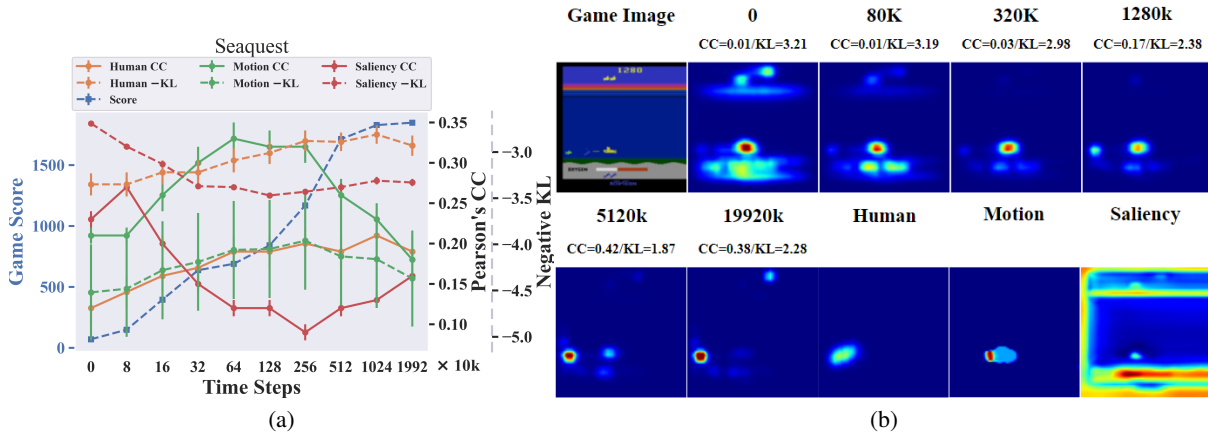


Figure 6. Seaquest: (a) Human and RL saliency maps becomes more similar according to the KL metric (yellow dashed line). Pearson's correlation coefficients between game score and human are CC: $r(8) = 0.824, p < 0.01$; KL: $r(8) = 0.930, p < 0.001$; between game score and motion are CC: $r(8) = -0.116, p = 0.750$, KL: $r(8) = 0.419, p = 0.228$; between game score and saliency are CC: $r(8) = -0.653, p < 0.05$, KL: $r(8) = -0.641, p < 0.05$. (b) The RL agents learn to attend to an incoming enemy on the left.

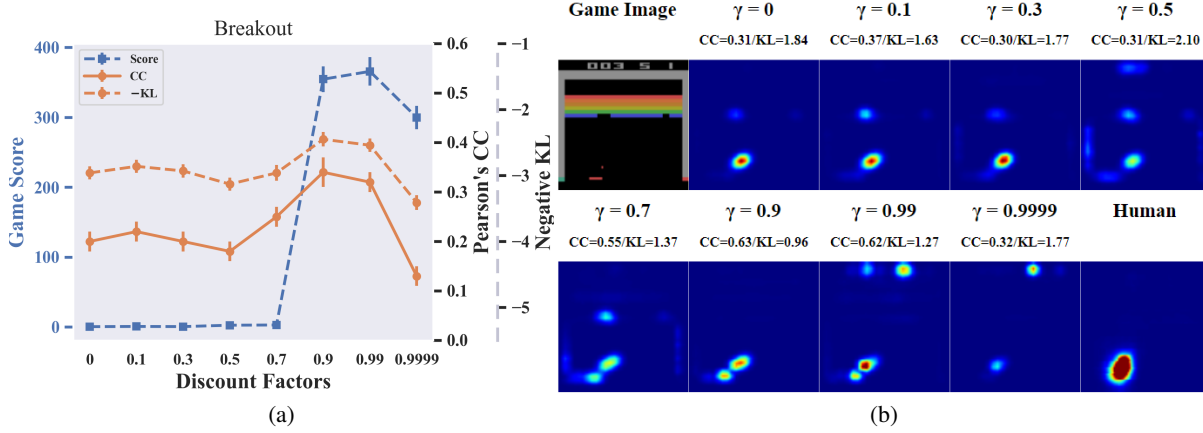


Figure 7. Breakout: (a) The RL agent’s attention is most similar to human’s when $\gamma = 0.9$. (b) Human attention is on the paddle and the ball. Setting $\gamma > 0.9$ makes the agent attend to the score at the top of the image.

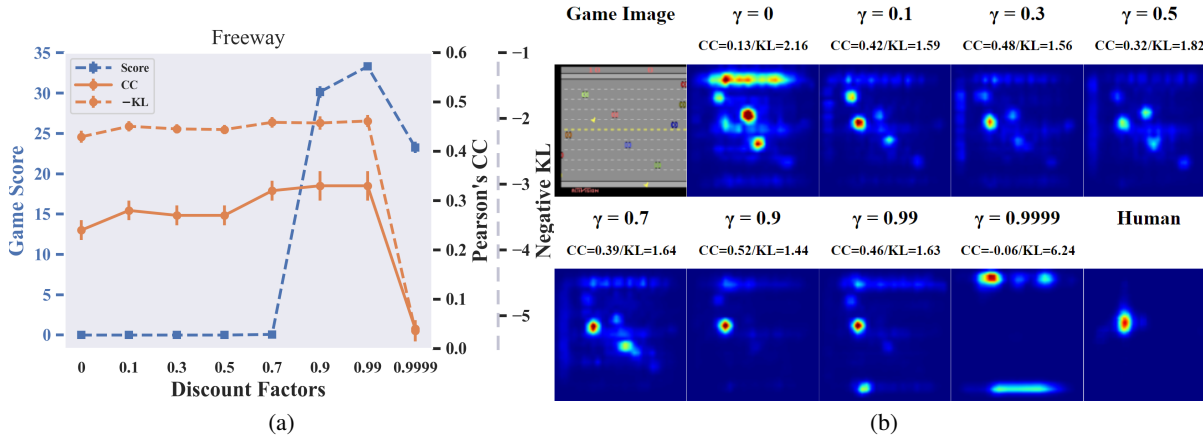


Figure 8. Freeway: (a) The RL agent’s attention is most similar to human’s when $\gamma = 0.9$ and $\gamma = 0.99$. (b) Human attention is on the yellow chicken being controlled to cross the highway.

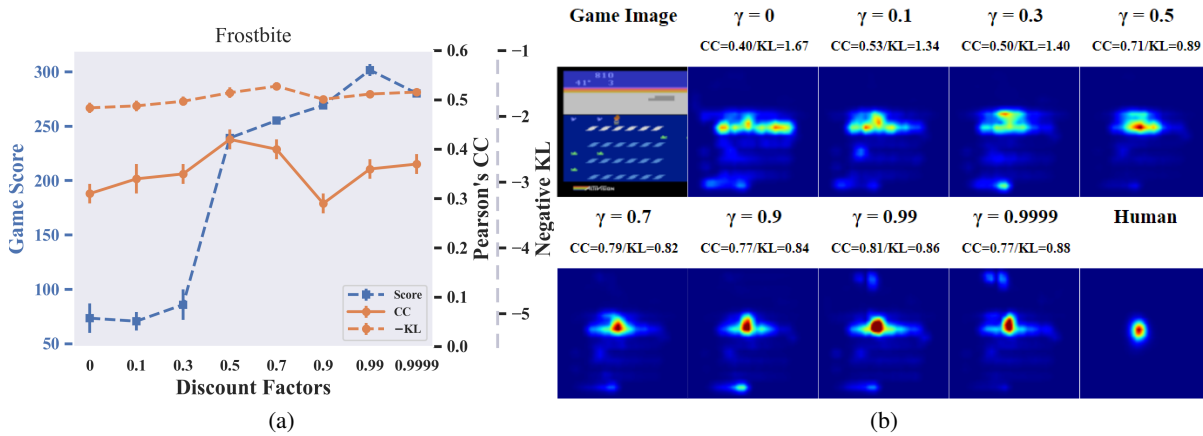


Figure 9. Frostbite: (a) The RL agent’s attention is most similar to human’s when $\gamma = 0.7$ (CC) or 0.5 (KL). (b) Human attention is on the little person being controlled in the middle.

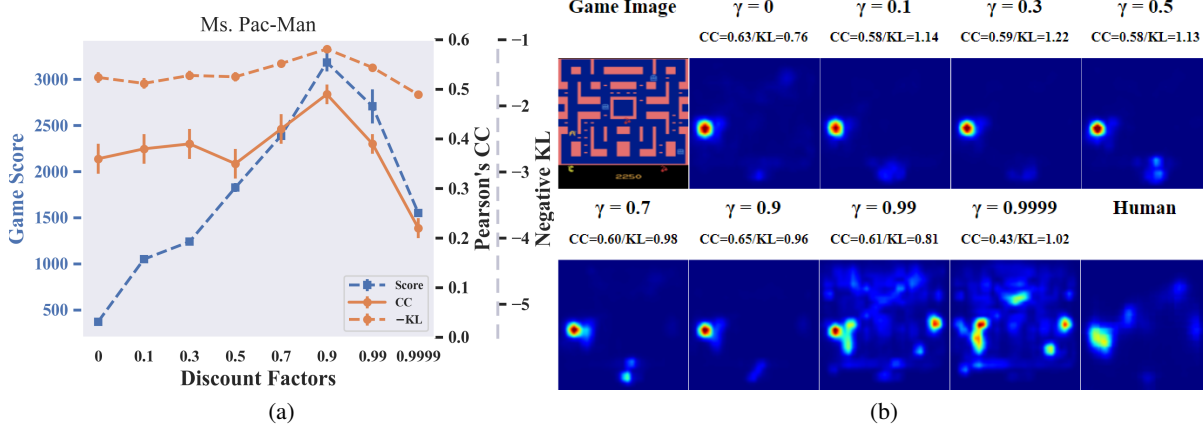


Figure 10. Ms. Pac-Man: (a) The RL agent’s attention is most similar to human’s when $\gamma = 0.9$. Note that choosing this value and deviating from the default $\gamma = 0.99$ lead to a better performance. (b) Human attention is mostly on the Pac-Man on the left side. Setting $\gamma > 0.9$ distracts the agent to attend to other objects.

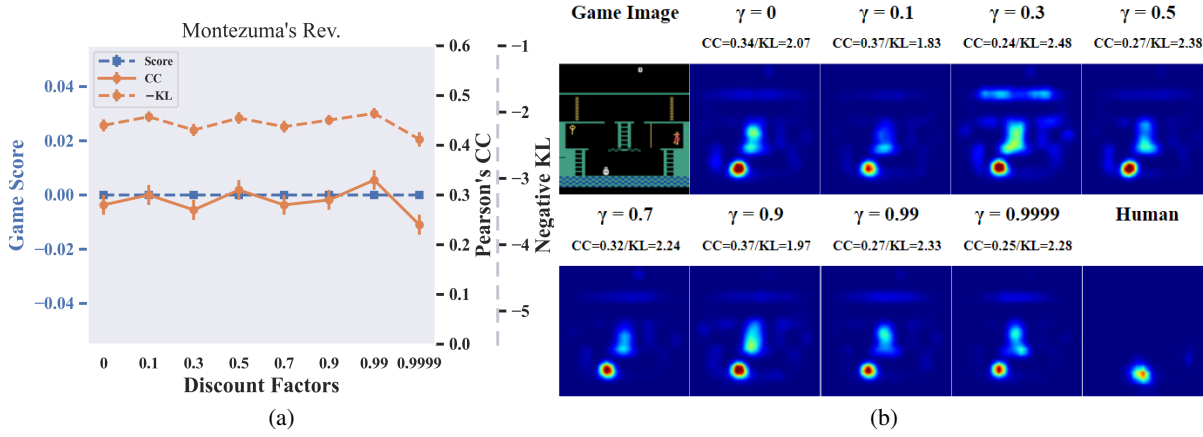


Figure 11. Montezuma's Revenge: (a) The RL agent’s attention is most similar to human’s when $\gamma = 0.99$. Note that this is a difficult game for RL agents and they never learn to score. (b) Human attention is on the enemy at the bottom.

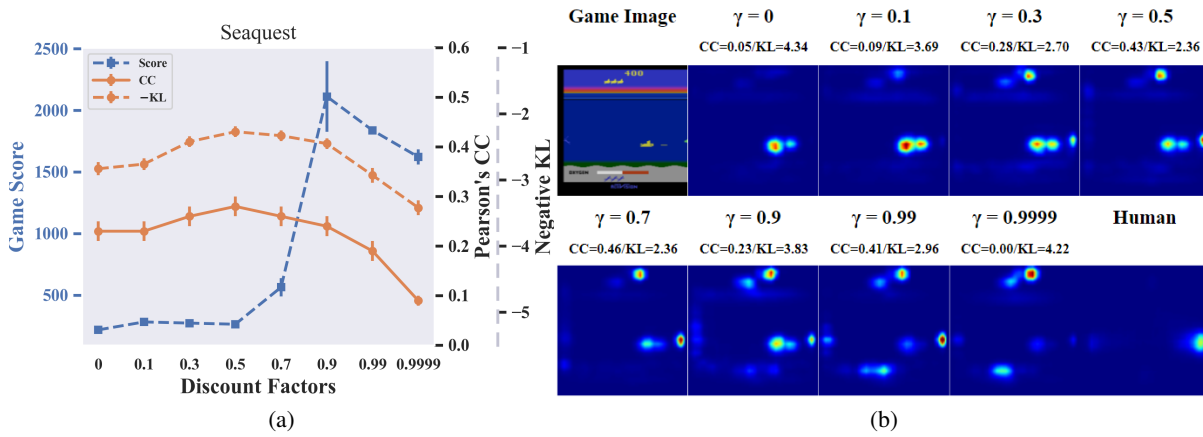


Figure 12. Seaquest: (a) The RL agent’s attention is most similar to human’s when $\gamma = 0.5$. Note that choosing $\gamma = 0.9$ and deviating from the default $\gamma = 0.99$ lead to a better performance. (b) Human attention is on an appearing enemy on the right side. With $\gamma > 0.9$ the RL agent also learns to attend to the oxygen bar at the bottom.

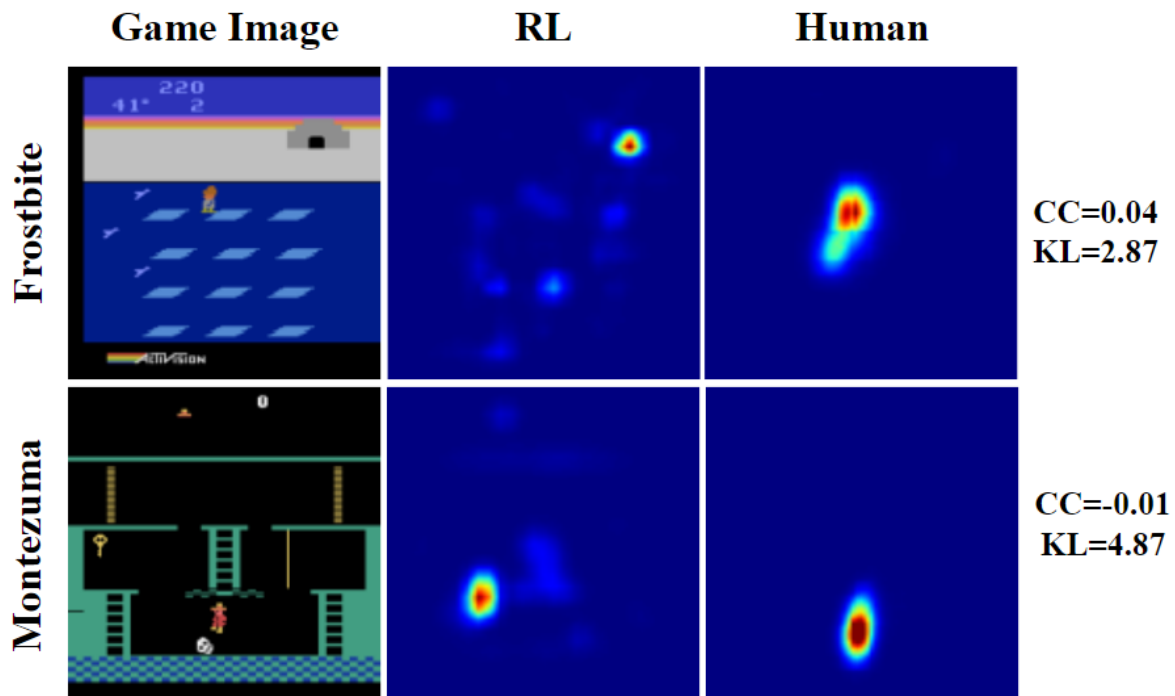


Figure 13. Games in which human attention and RL agents' attention are more different in the failure states than the normal states. This indicates that in these games the mistakes are likely caused by wrong attention which subsequently led to wrong decisions. Frostbite: The RL agent is attending to the entrance of the Igloo. It should attend to the little person in the middle like humans do to avoid an incoming enemy from the left. Montezuma's Revenge: The RL agent is attending to the bottom of the ladder. It should attend the little person and the enemy to escape from the dangerous situation.

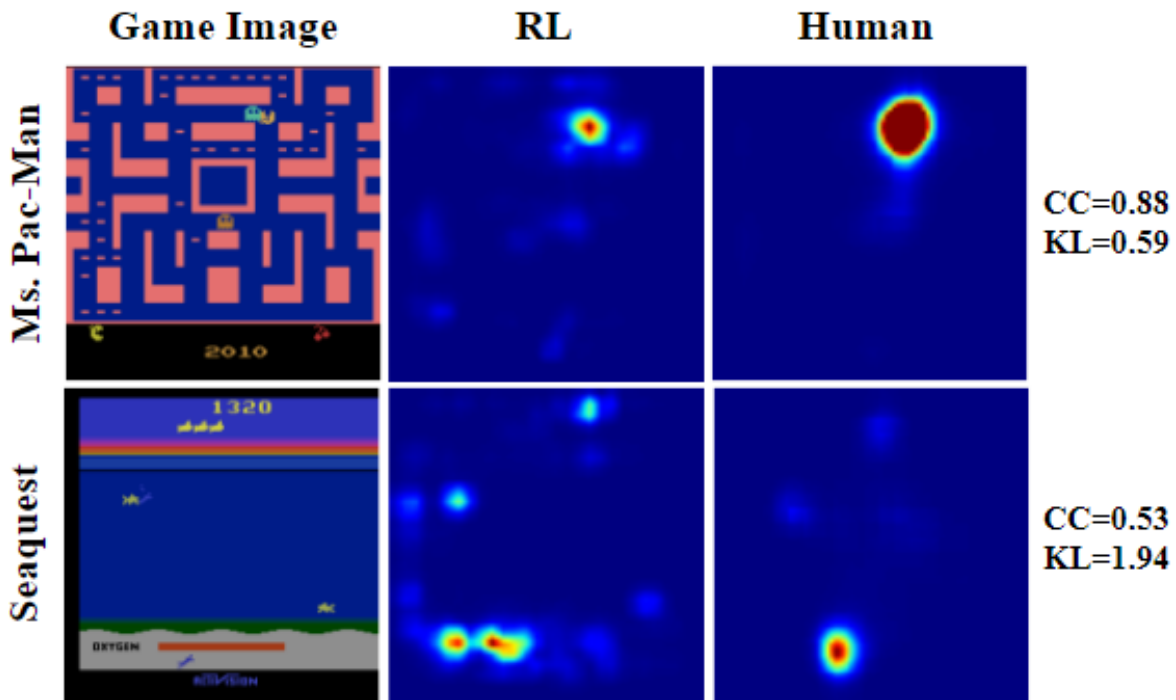


Figure 14. Games in which human attention and RL agents' attention are more similar in the failure states than the normal states. This suggests that they generally agree on the objects to be attended to. But the RL agents made wrong decisions due to its suboptimal policy. Ms.Pac-Man: The agent and the human both attend to the Pac-Man which is about to be captured by the cyan enemy ghost. The agent failed to run away from it. Seaquest: The agent and the human both attend to the empty oxygen bar at the bottom. The agent failed to refill oxygen before it runs out.

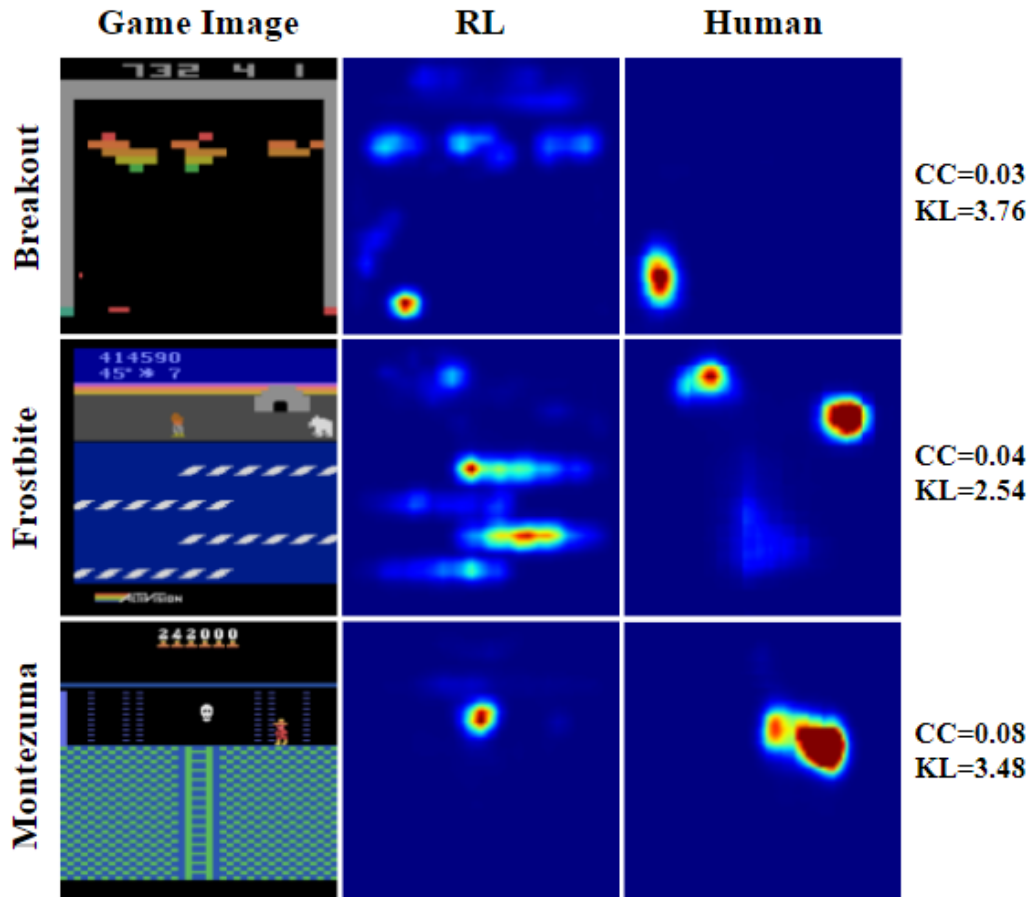


Figure 15. Games in which human attention and RL agents' attention are more different in unseen states than the normal states. This is mostly due to new objects that the agents have never encountered. Breakout: The CC value drops significantly due to unseen spatial layouts of the bricks. The KL does not change much because there are no new objects so the agent can still attend to human attended objects like the ball on the left. Frostbite: Human attention is around the polar bear (a new object) at the upper right corner. Montezuma's Revenge: Human attention is on the fire beacon (a new object). The RL agent's attention is on the skull which is a familiar object.

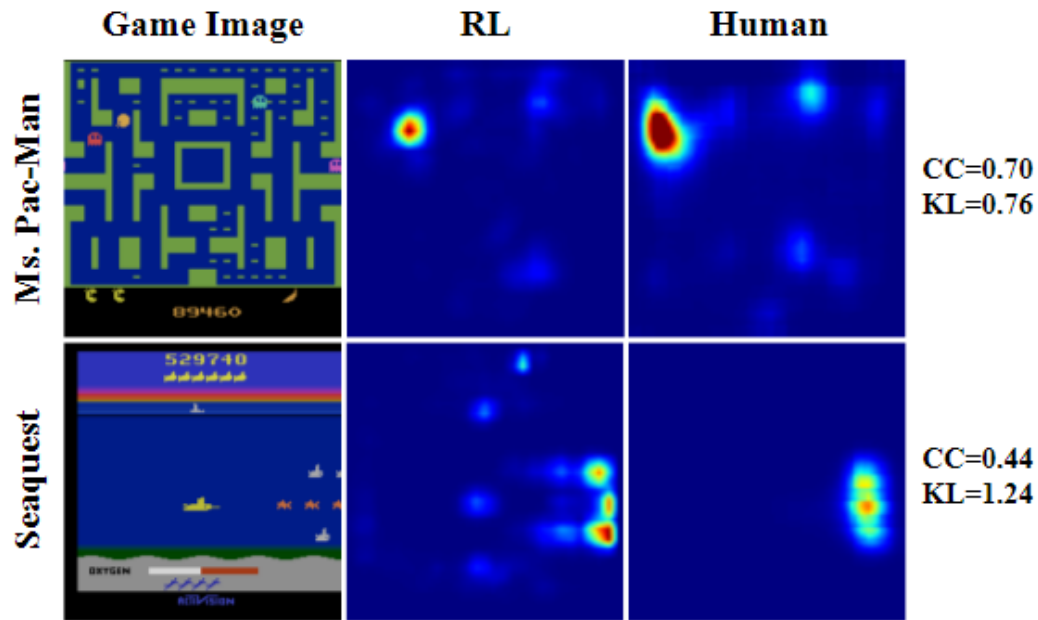


Figure 16. Games in which human attention and RL agents' attention are more similar in the unseen states than the normal states. This is because there are no new objects in these unseen states – objects move much faster and appear in larger numbers. The player often encounters dangerous states that are close to failure. As shown in Appendix Fig. 14 human attention and RL agent's attention are often similar in failure states for these two games. Ms. Pac-Man: The agent and the human both attend to the Pac-Man which is about to be captured by the red enemy ghost. Seaquest: The agent and the human both attend to the enemies on the right side.

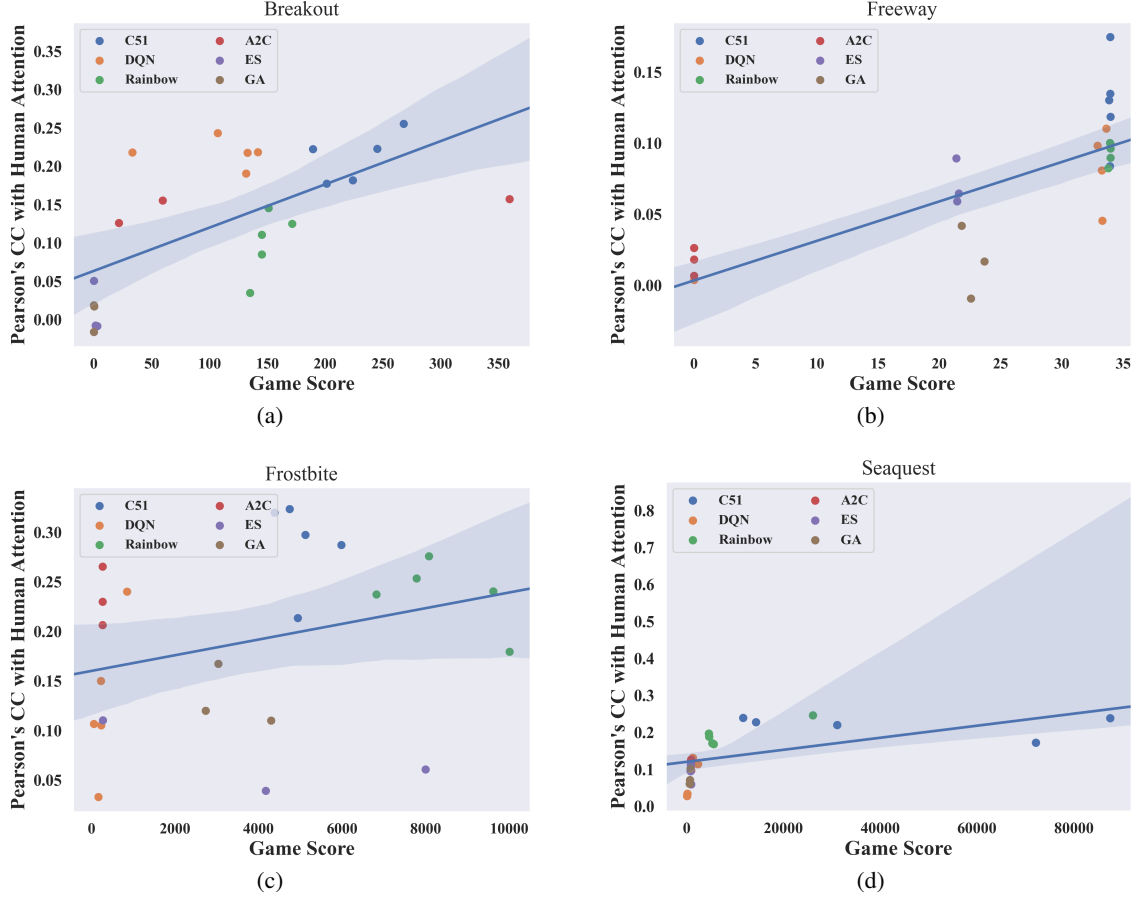


Figure 17. The relation between the similarity with human attention and algorithm's performance. The line shows the linear regression line fitted to the data point and the shaded area is the 95% confidence interval. The correlation coefficients between the similarity measurement and game score are: $r(22) = 0.634, p < 0.001$ for Breakout, $r(22) = 0.743, p < 0.001$ for Freeway, $r(22) = 0.298, p = 0.158$ for Frostbite, and $r(22) = 0.553, p < 0.01$ for Seaquest.